

Current Status of the CKM Matrix and the CP Violation

Achille Stocchi

Laboratoire de l'Accélérateur Linéaire,
IN2P3-CNRS et Université de Paris-Sud, Bât. 200, BP 34, 91898 Orsay Cedex, France

Abstract

These lectures give an introduction and the current status of flavour physics in the quark sector, with special attention to the CKM matrix and CP violation. We describe the measurements which contribute to the determination of the CKM matrix elements and how, together with important theoretical developments, they have significantly improved our knowledge on the flavour sector of the Standard Model. These lectures are complemented by the seminar of U. Mallik (see these proceedings) which describes in more details the most recent CP-violating related measurements by the B-factories. The results presented are up-to-date till winter 2004.

keywords :

CKM matrix, CP violation, Beauty (B) hadrons, B decays, Unitarity Triangle

Contents

1	Introduction	3
2	Short story: from strangeness to the CKM Matrix	3
3	The Standard Model in the fermion sector and the CKM matrix	5
4	The CKM Matrix	7
4.1	The Unitarity Triangle	9
4.2	General Introduction to Oscillation and CP Violation	10
4.3	Standard Model formulae relating $\overline{\rho}$ and $\overline{\eta}$ to experimental and theoretical inputs	13
5	B Physics at different facilities	17
6	Evaluation of the parameters entering in the determination of the CKM parameters.	18
6.1	Determination of $ V_{cb} $	18
6.1.1	Determination of $ V_{cb} $ using inclusive analyses	18
6.1.2	Determination of $ V_{cb} $ using $B \rightarrow D^* \ell \nu$ analyses	20
6.1.3	Determination of $ V_{cb} $ using inclusive and exclusive methods	20
6.2	Determination of $ V_{ub} $	20
6.2.1	Determination of $ V_{ub} $ using inclusive analyses	20
6.2.2	Determination of $ V_{ub} $ using exclusive analyses	21
6.2.3	Determination of $ V_{ub} $ using inclusive and exclusive methods	22
6.3	Measurements of $B^0 - \overline{B}^0$ oscillations	22
6.3.1	Measurements of the $B_d^0 - \overline{B}_d^0$ oscillation frequency: Δm_d	22
6.3.2	Search for $B_s^0 - \overline{B}_s^0$ oscillations	23
6.4	Some theoretical inputs: B_K , $f_B \sqrt{\hat{B}_B}$ and ξ	24
6.4.1	Brief introduction to Lattice QCD (LQCD)	25
6.5	Determination of $\sin(2\beta)$ from CP asymmetry in $J/\psi K^0$ decays.	27
7	Determination of the Unitarity Triangle parameters	27
7.1	Fundamental test of the Standard Model in the fermion sector	28
7.2	Determination of the Unitarity Triangle parameters : $\overline{\eta}$, $\overline{\rho}$, $\sin(2\beta)$, $\sin(2\alpha)$, γ	29
7.2.1	Indirect versus direct determination of the Unitarity Triangle angles	29
7.3	Determination of other important quantities	30
7.3.1	The expected distribution for Δm_s	30
7.3.2	Determination of $f_{B_d} \sqrt{\hat{B}_{B_d}}$ and \hat{B}_K	32
7.4	Evolution on the precision on $\overline{\rho}$ and $\overline{\eta}$ over the last 15 years	33
7.5	Dulcis in fundo : the new-comers	34
8	Conclusions	34
9	Acknowledgements	35

1 Introduction

Accurate studies of the production and decay properties of beauty and charm hadrons are exploiting a unique laboratory for testing the Standard Model in the fermion sector, for studying QCD in the non-perturbative regime and for searching for New Physics through virtual processes.

In the Standard Model, weak interactions among quarks are encoded in a 3×3 unitary matrix: the CKM matrix. The existence of this matrix conveys the fact that quarks, in weak interactions, act as linear combinations of mass eigenstates [1, 2].

The CKM matrix can be parametrized in terms of four free parameters which are measured in several physics processes.

In a frequently used parametrization, these parameters are named: λ , A , $\bar{\rho}$ and $\bar{\eta}^1$. The Standard Model predicts relations between the different processes which depend upon these parameters. CP violation is accommodated in the CKM matrix and its existence is related to $\bar{\eta} \neq 0$. The unitarity of the CKM matrix can be visualized as a triangle in the $(\bar{\rho}, \bar{\eta})$ plane. Several quantities, depending upon $\bar{\rho}$ and $\bar{\eta}$ can be measured and they must define compatible values for the two parameters, if the Standard Model is the correct description of these phenomena. Extensions of the Standard Model can provide different predictions for the position of the apex of the triangle, given by the $\bar{\rho}$ and $\bar{\eta}$ coordinates. The most precise determination of these parameters is obtained using B decays, $B^0 - \bar{B}^0$ oscillations and CP asymmetry in the B and in the K sectors.

Many additional measurements of B meson properties (mass, branching fractions, lifetimes...) are necessary to constrain the Heavy Quark theories [Operator Product Expansion (OPE) /Heavy Quark Effective Theory (HQET) /Lattice QCD (LQCD)] to allow for precise extraction of the CKM parameters. In addition, to be able to extract the Standard Model parameters, it is also necessary to control and measure the backgrounds, and to acquire a detailed understanding of the experimental apparatus. All these aspects are important because they propagate as systematic errors attached to the values extracted for the CKM parameters. For instance, the values and the uncertainties of the B hadron lifetimes enter in many important quantities. Experimental progress in various B physics measurements has been crucial in the determination of the CKM matrix elements. These last aspects are not treated in these lectures.

2 Short story: from strangeness to the CKM Matrix

The discovery of the strange particle in 1947 was totally unexpected and can be seen as the beginning of a new era in particle physics which has not ended yet. Just after the pion discovery by C.M.G. Lattes, H. Muirhead, C.F. Powell and G.P. Occhialini [4], in 1947, the same year, C.C. Butler and G.D. Rochester [5] reveal, having exposed a cloud chamber to cosmic rays, the existence of a still-heavier unstable particle decaying in a typical V-topology; this earlier name could be ascribed to the characteristic topology of the tracks which were produced when a neutral particle decays into two charged particles. At the same time there were also events in which a charged particle trajectory had a sharp break indicating a decay (V^\pm) (corresponding to the decay $K^+ \rightarrow \mu^+ \nu_\mu$).

In fact, the first example of such particles was reported by L. Leprince-Ringuet and M. Lh eritier in 1944 [6]. They observed a secondary cosmic ray particle, in a cloud chamber placed at the Laboratoire de l'Argent iere (Hautes-Alpes), producing a recoil electron (energetic delta ray). From the measured curvatures of the ongoing and outgoing particles and using the value of the scattering angle of the electron it was possible to determine the mass of the incident particle which was found to be of $495 \pm 60 \text{ MeV}/c^2$. It is today clear that this particle is the charged Kaon, nevertheless this discovery came too early, since even the pion was not discovered at that time!

It took two years to confirm the result of Rochester and Butler. These experiments were continued at higher altitude and with high degree of precision [7]. The results unambiguously established the existence of two states: $\Lambda \rightarrow p\pi^-$ and $K^0 \rightarrow \pi^+\pi^-$. In 1953 it became possible to produce those V-particles

¹ $\bar{\rho} = \rho(1 - \frac{\lambda^2}{2})$; $\bar{\eta} = \eta(1 - \frac{\lambda^2}{2})$ [3].

in accelerators² and it was then clear that they were produced in reactions mediated by the strong interaction; furthermore those particles were always produced in pairs (*associated production*). On the other hand their typical lifetime was of about 10^{-10} s which is a typical time scale of the weak interaction³. These particles are then “strange”, as they are produced through the strong interaction whereas they decay through weak interaction processes. The solution was proposed, after several unfruitful tentative, by M. Gell-Mann [8], to introduce a new additive quantum number: the *strangeness*⁴. The strangeness was assigned to be -1 for the Λ , the \bar{K}^0 and the K^- (and +1 for the corresponding antiparticles), -2 for the Ξ^- and 0 for all non-strange particles and making the hypothesis that this new quantum number is conserved by strong and electromagnetic interactions and is not conserved by the weak interaction. This allows to “explain”, a posteriori, why strange particles are always produced in pairs (by strong interactions $\Delta S=0$) and have a relatively long lifetime (decay through weak interactions $\Delta S=1$).

In the decay, the strangeness changes by one unit and these transitions were classified as $\Delta S = 1$. An intense experimental activity on strange particles shown, in the fifties, that the absolute decay rate for these transitions was suppressed by a factor of about 20 as compared with the corresponding rate measured in $\Delta S = 0$ decays.

In the early 60’s the existence of new constituents of matter was postulated: they were called quarks. They were independently introduced by M. Gell-Mann[9] and G. Zweig [10] and they should transform according to the fundamental representation of SU(3). They were supposed to have spin 1/2 and to exist in three varieties: the quark u with charge $+2/3$, the quarks d and s with charge $-1/3$. By analogy with leptons it was suggested that the quarks were also organized into doublets and the existence of a new quark of charge $2/3$ was proposed [11].

In 1963, N. Cabibbo proposed [1] a model to account for the suppression of $\Delta S=1$ transitions. In this model the d and s quarks, involved in weak processes, are rotated by a mixing angle θ_c : the Cabibbo angle. The quarks are organized in a doublet:

$$\begin{pmatrix} u \\ d_c \end{pmatrix} = \begin{pmatrix} u \\ d \cos\theta_c + s \sin\theta_c \end{pmatrix} \quad (1)$$

the small value of $\sin \theta_c$ ($\simeq 0.22$) is responsible for the suppression of strange particle decays (the coupling being proportional to $\sin^2\theta_c$). In this picture the slight suppression of $n \rightarrow p e^- \bar{\nu}_e$ with respect to the rate of $\mu^- \rightarrow e^- \nu_\mu \bar{\nu}_e$ is also explained by the fact that the coupling in the neutron decay is proportional to $\cos^2\theta_c$.

In this model, the neutral current coupling can be written⁵:

$$u\bar{u} + d\bar{d} \cos^2\theta_c + s\bar{s} \sin^2\theta_c + (s\bar{d} + d\bar{s}) \cos\theta_c \sin\theta_c. \quad (2)$$

The presence of the $(s\bar{d} + d\bar{s})$ term implies the existence of a flavour changing neutral current (FCNC). This was a serious problem for the Cabibbo model, since these couplings would produce contributions to Δm_K and $K_L \rightarrow \mu^+ \mu^-$ decays which are larger by several order of magnitude.

In 1970 S. Glashow, J. Iliopoulos and L. Maiani [12] (GIM) proposed the introduction of a new quark, named c , of charge $2/3$ and the introduction of a new doublet of quarks formed by the c quark and by a combination of the s and d quarks orthogonal to d_c (eq. 1):

$$\begin{pmatrix} c \\ s_c \end{pmatrix} = \begin{pmatrix} c \\ s \cos\theta_c - d \sin\theta_c \end{pmatrix}. \quad (3)$$

²The Brookhaven 3 GeV Cosmotron was the first accelerator delivering strange particles, followed by the Berkeley 6 GeV Bevatron.

³The scattering cross section of events like $\pi^- p \rightarrow K^0 \Lambda$ corresponds to the geometrical cross section of hadrons ($\simeq 10^{-13}$ cm²) which indicates that the Λ and the K^0 are produced through strong interactions. The natural lifetime of the strong interaction can be estimated using the relationship $\tau_{st} = (had.radius)/c \simeq 10^{-23}$ s.

⁴The observation of events such as $\Xi^- \rightarrow \Lambda \pi^-$, the so-called cascade events, and the non-observation of events such as $\Xi^- \rightarrow n \pi^-$, closed up the option that the *strangeness* could be a multiplicative quantum number (a kind of “strange parity”) being +1 for strange particles and -1 for non-strange ones. It was in fact the first indication of the existence of double strange particles.

⁵More formally. The charged currents are described by the operators $J_\mu^{+(-)}$. The existence of the neutral current is needed to complete the group algebra (obtained by commuting the operators J_μ^+ and J_μ^-) and necessarily contains $\Delta S=\pm 1$ terms.

In this way the $(s\bar{d} + d\bar{s})$ term (in Eq. 2), in the neutral current, is cancelled.

The discovery of the charm quark in the form of $c\bar{c}$ bound states [13] and the observation of charmed particles decaying into strange particles [14] (the $c\bar{s}$ transitions which are proportional to $\cos^2\theta_c$ dominate over the $c\bar{d}$ transitions which are proportional to $\sin^2\theta_c$) represent a tremendous triumph of this picture.

It should be reminded that a candidate event for the decay of a charm hadron was first observed in 1971, in Japan, in an emulsion detector exposed to cosmic rays [15]: $X^\pm \rightarrow h^\pm\pi^0$. The lifetime of h^\pm and its mass were found to be 10^{-14} sec and 1.8 GeV respectively ! (see [16] and [17] for more details).

The charge current, mediated by the emission of a W boson, can then be written:

$$(\bar{u}\bar{c})\gamma^\mu(1 - \gamma_5)V \begin{pmatrix} d \\ s \end{pmatrix} \quad (4)$$

where $\gamma^\mu(1 - \gamma_5)$ is the $V - A$ current, which accounts also for parity violation, u, d, s, c are the mass eigenstates and V is defined as:

$$V = \begin{pmatrix} \cos\theta_c & \sin\theta_c \\ -\sin\theta_c & \cos\theta_c \end{pmatrix}. \quad (5)$$

V is the Cabibbo unitary matrix which specifies the quark states which are involved in weak interactions. In 1975 the Mark I group at SPEAR discovered the third charged lepton: the τ [18]. Two years later the fifth quark, the b , was found at FNAL [19]. The indirect existence for the top quark t from the observation of $B_d^0 - \bar{B}_d^0$ oscillations [20] suggested the existence of an heavier version of the doublets (u, d) and (c, s) ⁶. The t quark was finally discovered in 1995 at Fermilab [21] in $p\bar{p}$ collisions.

The existence of three quark doublets was already proposed by M. Kobayashi and K. Maskawa in 1973 [2] as a possible explanation for CP violation. Their proposal is a generalization of the Cabibbo rotation and implies that the weak flavour changing transitions are described by a 3×3 unitary matrix:

$$\begin{pmatrix} u \\ c \\ t \end{pmatrix} \rightarrow V \begin{pmatrix} d \\ s \\ b \end{pmatrix}, \quad V = \begin{pmatrix} V_{ud} & V_{us} & V_{ub} \\ V_{cd} & V_{cs} & V_{cb} \\ V_{td} & V_{ts} & V_{tb} \end{pmatrix}. \quad (6)$$

This matrix conveys the fact that there is an arbitrary rotation, usually applied to the -1/3 charged quarks, which is due to the mismatch between the strong and the weak eigenstates. This matrix can be parametrized using three real parameters and one phase which cannot be removed by redefining the quark field phases. This phase leads to the violation of the CP symmetry. In fact since CPT is a good symmetry for all quantum field theories, the complexity of the Hamiltonian implies that the time reversal invariance T and thus CP is violated⁷. In this picture the Standard Model includes CP violation in a simple way.

3 The Standard Model in the fermion sector and the CKM matrix

The Standard Model is based on the $SU(2)_L \times U(1)_Y$ gauge symmetry, where the index L stands for left, since only the *left* handed particles are implied in the charged weak current. In a Lagrangian the mass term of a fermionic field is of the type⁸

$$m\bar{\psi}\psi = m(\bar{\psi}_R\psi_L + \bar{\psi}_L\psi_R). \quad (7)$$

⁶Another indirect piece of evidence for the existence of top was the measurement of the Z^0 coupling to a $b\bar{b}$ pairs, which shown that the b quark is a member of an doublet with partner that cannot be a u or a c quark.

⁷The time is an anti-linear operator: $T(\lambda_1|\psi_1\rangle + \lambda_2|\psi_2\rangle) = \lambda_1^*T|\psi_1\rangle + \lambda_2^*T|\psi_2\rangle$. It can be simply understood, recalling that $\psi(x, t)$ and $\psi^*(x, -t)$ (and not $\psi(x, -t)$) obey to the same Schrodinger equation. If the operator T is applied to the Standard Model Lagrangian and thus to the CKM matrix: $T V(CKM)|\dots\rangle = V^*(CKM) T|\dots\rangle$. If $V(CKM)$ is complex, $V(CKM) \neq V(CKM)^*$. In this case the Hamiltonian does not commute with T, thus T is not conserved and, since CPT is conserved, CP is violated.

⁸The Euler-Lagrange equation implies the following correspondence between motion equations and Lagrangians:
 $\mathcal{L} = \delta^\mu\psi\delta_\mu\psi - 1/2m^2\psi^2 \rightarrow (\delta_0\delta^0 + m^2)\psi \rightarrow (E^2 = p^2 + m^2)$ (Einstein equation).
 $\mathcal{L} = i\psi\gamma_0\delta^0\psi - m\bar{\psi}\psi \rightarrow (i\gamma^0 - m)\psi = 0$ (Dirac equation).

Thus the mass implies a *left-right* coupling⁹ which is not gauge invariant. An economical approach for introducing fermion masses, in a gauge-invariant way, is to consider Yukawa couplings in which contributes a weak iso-doublet field ϕ :

$$\bar{\psi}_L \phi \psi_R ; \text{ with } \quad \phi = \begin{pmatrix} \phi^+ \\ \phi^0 \end{pmatrix}, \quad I_\phi = 1/2, \quad Y_\phi = 1, \quad (8)$$

where the quantum numbers of the new doublet (ϕ) are exactly those needed to restore the gauge invariance of the interaction vertex giving the mass to fermions.

In the Standard Model, the Lagrangian corresponding to charged weak interactions can be written as:

$$\mathcal{L}_W = \frac{g}{2} \bar{Q}_{L_i}^{Int.} \gamma^\mu \sigma^a Q_{L_i}^{Int.} W_\mu^a ; \quad Q_{L_i}^{Int.} = \begin{pmatrix} u_{L_i} \\ d_{L_i} \end{pmatrix}, \quad L_{L_i}^{Int.} = \begin{pmatrix} \nu_{L_i} \\ \ell_{L_i} \end{pmatrix}, \quad (9)$$

the index *Int.* indicates the weak interaction basis, σ^a are the Pauli matrices (a=1,2,3), W_μ^a are the $SU(2)_L$ gauge bosons and i is the quark index. It can be noted that: $\bar{Q}_{L_i}^{Int.} Q_{L_i}^{Int.} = \bar{Q}_{L_i}^{Int.} \mathbf{1}_{ij} Q_{L_j}^{Int.}$. The charged weak interactions are family blind (the quantum numbers of the Standard Model are I_3 and Y which do not “feel” the family index).

In the interaction basis the Yukawa interaction is:

$$\mathcal{L}_Y = Y_{ij}^d \bar{Q}_{L_i}^{Int.} \phi d_{R_j}^{Int.} + Y_{ij}^u \bar{Q}_{L_i}^{Int.} \tilde{\phi} u_{R_j}^{Int.} + Y_{ij}^\ell \bar{L}_{L_i}^{Int.} \phi \ell_{R_j}^{Int.} + H.C. , \quad (10)$$

where $\tilde{\phi} = i\sigma_2 \phi^*$. In the most general case the matrices Y_{ij} are complex.

The presence of two independent matrices Y_{ij} , for the *up*-type and *down*-type quark, is due to the behaviour of the Yukawa coupling itself.

After spontaneous symmetry breaking (SSB):

$$\phi = \frac{1}{\sqrt{2}} \begin{pmatrix} 0 \\ v \end{pmatrix}, \quad (11)$$

and the Yukawa interaction can be written:

$$\mathcal{L}_M = \bar{d}_{L_i}^{Int.} M_{ij}^d d_{R_j}^{Int.} + \bar{u}_{L_i}^{Int.} M_{ij}^u u_{R_j}^{Int.} + \bar{\ell}_{L_i}^{Int.} M_{ij}^\ell \ell_{R_j}^{Int.} + H.C. \quad (12)$$

where $M^u = (v/\sqrt{2})Y^u$ and $M^d = (v^*/\sqrt{2})Y^d$. Physical masses are obtained by finding transformations of the fields such that the corresponding mass matrices become real and diagonal:

$$M^f(diag) = V_L^f M^f (V_R^f)^\dagger . \quad (13)$$

Therefore, the mass eigenstates are

$$\begin{aligned} d_{L_i} &= (V_L^d)_{ij} d_{L_j}^{Int.} ; & d_{R_i} &= (V_R^d)_{ij} d_{R_j}^{Int.} \\ u_{L_i} &= (V_L^u)_{ij} u_{L_j}^{Int.} ; & u_{R_i} &= (V_R^u)_{ij} u_{R_j}^{Int.} \\ \ell_{L_i} &= (V_L^\ell)_{ij} \ell_{L_j}^{Int.} ; & \ell_{R_i} &= (V_R^\ell)_{ij} \ell_{R_j}^{Int.} \\ & & \nu_{L_i} &= (V_L^\nu)_{ij} \nu_{L_j}^{Int.} \end{aligned} \quad (14)$$

In this basis the Lagrangian for the weak interaction can be written as:

$$\mathcal{L}_W = \frac{g}{2} \bar{u}_{L_i} \gamma^\mu [V_L^u (V_L^d)^\dagger] d_{L_j} W_\mu^a + h.c. \quad (15)$$

where

$$V(CKM) = V_L^u (V_L^d)^\dagger . \quad (16)$$

⁹It simply follows from the properties of projection operators and using the equalities $\bar{\psi}_R = \bar{\psi} P_L$ and $\bar{\psi}_L = \bar{\psi} P_R$. It follows that:

$m \bar{\psi} \psi = m \bar{\psi} (P_L + P_R) \psi = m \bar{\psi} (P_L P_L + P_R P_R) \psi = m [(\bar{\psi} P_L)(P_L \psi) + (\bar{\psi} P_R)(P_R \psi)] = m (\bar{\psi}_R \psi_L + \bar{\psi}_L \psi_R)$

$V(\text{CKM})$ is the CKM matrix. The phenomenon of flavour changing can be appreciated in two different ways (different basis). If we use the basis in which the mass matrices are diagonal, the Lagrangian for the interactions is not anymore family blind. The interaction among quarks belonging to different families are possible and the couplings are encoded in the CKM matrix.

If the same procedure is applied in the lepton sector it follows that:

$$V(\text{leptons}) = (V_L^\nu (V_L^\ell)^\dagger) = (V_L^\ell (V_L^\ell)^\dagger) = 1, \quad (17)$$

since the mass matrix of the neutrinos is arbitrary (the neutrinos are massless in the SM), we can always choose $V_L^\nu = V_L^\ell$.

There is freedom in parametrising the CKM matrix:

- a permutation between the different generations (it is normally chosen to order the quarks by increasing value of their mass (u, c, t and d, s, b)),
- the presence of phases in the CKM matrix. It is clear that $M(\text{diag})$ is unchanged if the matrices $V_{L(R)}$ are multiplied by a matrix containing only phases: $\tilde{V}_{L(R)}^f = P^f V_{L(R)}^f$, it follows $V(\text{CKM}) = P^u V(\text{CKM}) P^{*d}$.

As long as some of these phases are not observable, one has to require that the CKM matrix contains the minimal number of phases, all the others being absorbed in the definition of quark wave functions.

The 2×2 matrix can be used to illustrate the contribution of these arbitrary phases in the CKM matrix:

$$\begin{aligned} V = \begin{pmatrix} V_{11} & V_{12} \\ V_{21} & V_{22} \end{pmatrix} &\rightarrow \begin{pmatrix} e^{-i\phi_1} & 0 \\ 0 & e^{-i\phi_2} \end{pmatrix} \begin{pmatrix} V_{11} & V_{12} \\ V_{21} & V_{22} \end{pmatrix} \begin{pmatrix} e^{+i\chi_1} & 0 \\ 0 & e^{+i\chi_2} \end{pmatrix} \\ &= \begin{pmatrix} V_{11}e^{-i(\phi_1-\chi_1)} & V_{12}e^{-i(\phi_1-\chi_2)} \\ V_{21}e^{-i(\phi_2-\chi_1)} & V_{22}e^{-i(\phi_2-\chi_2)} \end{pmatrix} \end{aligned} \quad (18)$$

It can be noted that:

$$(\phi_2 - \chi_2) = (\phi_2 - \chi_1) + (\phi_1 - \chi_2) - (\phi_1 - \chi_1) \quad (19)$$

Among the four phases, corresponding to the four quark flavours, only three can be chosen in an arbitrary way, since one phase difference is obtained as a linear sum of the other three. In the general case, the number of arbitrary phases is: $2n(\text{families}) - 1$.

The CKM matrix is a rotation matrix and, in a complex plane, can be parametrized in terms of a given number of angles (real numbers) and phases (complex numbers) as indicated in Table 1.

Family of quarks	num. of Angles	num. Phases	Irreducible Phases
n	$n(n-1)/2$	$n(n+1)/2$	$n(n-1)/2 - (2n-1)$ $= (n-1)(n-2)/2$
2	1	3	0
3	3	6	1
4	6	10	3

Table 1: *Numbers of angles and phases parametrising a complex rotation matrix. The last column gives the number of phases which cannot be reabsorbed into the quark fields.*

It results that a 2×2 matrix (the Cabibbo matrix) is parametrized in terms of one real parameter and contains no phase. The 3×3 matrix (CKM) is parametrised in terms of three real parameters and one irreducible phase. The presence of this complex number in the Lagrangian, as explained at the end of Section 2 (footnote 7), is responsible, and it is the only one, of the fact that the CP symmetry is violated in the Standard Model.

4 The CKM Matrix

Many parametrizations of the CKM matrix have been proposed in the literature. The most popular are the standard parametrization [22] recommended by [23] and a generalization of the Wolfenstein parametrization [24] as presented in [3].

With $c_{ij} = \cos \theta_{ij}$ and $s_{ij} = \sin \theta_{ij}$ ($i, j = 1, 2, 3$), the standard parametrization is given by:

$$V_{\text{CKM}} = \begin{pmatrix} c_{12}c_{13} & s_{12}c_{13} & s_{13}e^{-i\delta} \\ -s_{12}c_{23} - c_{12}s_{23}s_{13}e^{i\delta} & c_{12}c_{23} - s_{12}s_{23}s_{13}e^{i\delta} & s_{23}c_{13} \\ s_{12}s_{23} - c_{12}c_{23}s_{13}e^{i\delta} & -s_{23}c_{12} - s_{12}c_{23}s_{13}e^{i\delta} & c_{23}c_{13} \end{pmatrix}, \quad (1)$$

where δ is the phase necessary for CP violation. c_{ij} and s_{ij} can all be chosen to be positive and δ may vary in the range $0 \leq \delta \leq 2\pi$. However, measurements of CP violation in K decays force δ to be in the range $0 < \delta < \pi$. s_{13} and s_{23} are small numbers: $\mathcal{O}(10^{-3})$ and $\mathcal{O}(10^{-2})$, respectively. Consequently, from phenomenological applications, the four independent parameters are taken to be:

$$s_{12} = |V_{us}|, \quad s_{13} = |V_{ub}|, \quad s_{23} = |V_{cb}|, \quad \delta. \quad (2)$$

The first three quantities can be extracted from tree level decays mediated by the $s \rightarrow u$, $b \rightarrow u$ and $b \rightarrow c$ transitions, respectively. The phase δ can be obtained from CP violating or loop processes sensitive to the V_{td} matrix element.

The absolute values of the elements of the CKM matrix show a hierarchical pattern with the diagonal elements being close to unity: $|V_{us}|$ and $|V_{cd}|$ being of order 0.2, $|V_{cb}|$ and $|V_{ts}|$ of order $4 \cdot 10^{-2}$ and $|V_{ub}|$ and $|V_{td}|$ of order $5 \cdot 10^{-3}$. The Wolfenstein parametrization is useful to illustrate this structure. It shows that the matrix is almost diagonal, namely that the coupling between quarks of the same family is close to unity, and is decreasing as the separation between families increases:

$$V_{CKM} = \begin{pmatrix} 1 - \frac{\lambda^2}{2} & \lambda & A\lambda^3(\rho - i\eta) \\ -\lambda & 1 - \frac{\lambda^2}{2} & A\lambda^2 \\ A\lambda^3(1 - \rho - i\eta) & -A\lambda^2 & 1 \end{pmatrix} + \mathcal{O}(\lambda^4). \quad (3)$$

The set (2) is replaced by:

$$\lambda, \quad A, \quad \rho, \quad \eta, \quad (4)$$

known as the Wolfenstein parameters. To obtain the exact expression of the CKM parameters in the Wolfenstein parametrization, it is convenient to go back to the standard parametrization and to make the following change of variables in (1) [3, 25]:

$$s_{12} = \lambda, \quad s_{23} = A\lambda^2, \quad s_{13}e^{-i\delta} = A\lambda^3(\rho - i\eta). \quad (5)$$

At order λ^5 , the obtained CKM matrix in the extended Wolfenstein parametrization is:

$$V_{CKM} = \begin{pmatrix} 1 - \frac{\lambda^2}{2} - \frac{\lambda^4}{8} & \lambda & A\lambda^3(\rho - i\eta) \\ -\lambda + \frac{A^2\lambda^5}{2}(1 - 2\rho) - iA^2\lambda^5\eta & 1 - \frac{\lambda^2}{2} - \lambda^4\left(\frac{1}{8} + \frac{A^2}{2}\right) & A\lambda^2 \\ A\lambda^3\left[1 - \left(1 - \frac{\lambda^2}{2}\right)(\rho + i\eta)\right] & -A\lambda^2\left(1 - \frac{\lambda^2}{2}\right)\left[1 + \lambda^2(\rho + i\eta)\right] & 1 - \frac{A^2\lambda^4}{2} \end{pmatrix} + \mathcal{O}(\lambda^6). \quad (6)$$

By definition, the expression for V_{ub} remains unchanged relative to the original Wolfenstein parametrization and the corrections to V_{us} and V_{cb} appear only at $\mathcal{O}(\lambda^7)$ and $\mathcal{O}(\lambda^8)$, respectively. The advantage of this generalization of the Wolfenstein parametrization, over other generalizations found in the literature, is the absence of relevant corrections in V_{us} , V_{cd} , V_{ub} and V_{cb} . It can be noted that the element V_{td} can be re-expressed as:

$$V_{td} = A\lambda^3(1 - \bar{\rho} - i\bar{\eta})$$

where [3]

$$\bar{\rho} = \rho\left(1 - \frac{\lambda^2}{2}\right), \quad \bar{\eta} = \eta\left(1 - \frac{\lambda^2}{2}\right). \quad (7)$$

This elegant change in V_{td} , with respect to the original Wolfenstein parametrization, allows a simple generalization of the so-called unitarity triangle to higher orders in λ [3] as discussed below.

4.1 The Unitarity Triangle

From the unitarity of the CKM matrix ($VV^\dagger = V^\dagger V = 1$), non diagonal elements of the matrix products corresponding to six equations relating its elements can be written. In particular, in transitions involving b quarks, the scalar product of the third column with the complex conjugate of the first row must vanish:

$$V_{ud}^* V_{ub} + V_{cd}^* V_{cb} + V_{td}^* V_{tb} = 0 \quad (8)$$

$$\begin{array}{rcl}
 V_{ud}^* V_{us} + V_{cd}^* V_{cs} + V_{td}^* V_{ts} = 0 & \lambda & \lambda & \lambda^5 \\
 \boxed{V_{ub}^* V_{ud} + V_{cb}^* V_{cd} + V_{tb}^* V_{td} = 0} & \lambda^3 & \lambda^3 & \lambda^3 \\
 V_{us}^* V_{ub} + V_{cs}^* V_{cb} + V_{ts}^* V_{tb} = 0 & \lambda^4 & \lambda^2 & \lambda^2 \\
 V_{ud}^* V_{td} + V_{us}^* V_{ts} + V_{ub}^* V_{tb} = 0 & \lambda^3 & \lambda^3 & \lambda^3 \\
 V_{td}^* V_{cd} + V_{ts}^* V_{cs} + V_{tb}^* V_{cb} = 0 & \lambda^4 & \lambda^2 & \lambda^2 \\
 V_{ud}^* V_{cd} + V_{us}^* V_{cs} + V_{ub}^* V_{cb} = 0 & \lambda & \lambda & \lambda^5
 \end{array}$$

Figure 1: The six triangle equations from the unitarity condition of the CKM matrix.

Using the parametrization given in Equation (6), and neglecting contributions of order $\mathcal{O}(\lambda^7)$, the different terms, in this expression, are respectively:

$$\begin{aligned}
 V_{ud}V_{ub}^* &= A\lambda^3(\bar{\rho} + i\bar{\eta}), \\
 V_{cd}V_{cb}^* &= -A\lambda^3, \\
 V_{td}V_{tb}^* &= A\lambda^3(1 - \bar{\rho} - i\bar{\eta})
 \end{aligned} \quad (9)$$

The three expressions are proportional to $A\lambda^3$, which can be factored out, and the geometrical representation of Eq. (8), in the $(\bar{\rho}, \bar{\eta})$ plane, is a triangle with summit at $C(0, 0)$, $B(1, 0)$ and $A(\bar{\rho}, \bar{\eta})$.

- The lengths CA and BA , to be denoted respectively by R_b and R_t , are given by

$$\overline{AC} \equiv R_b \equiv \frac{|V_{ud}V_{ub}^*|}{|V_{cd}V_{cb}^*|} = \sqrt{\bar{\rho}^2 + \bar{\eta}^2} = \left(1 - \frac{\lambda^2}{2}\right) \frac{1}{\lambda} \left| \frac{V_{ub}}{V_{cb}} \right|, \quad (10)$$

$$\overline{AB} \equiv R_t \equiv \frac{|V_{td}V_{tb}^*|}{|V_{cd}V_{cb}^*|} = \sqrt{(1 - \bar{\rho})^2 + \bar{\eta}^2} = \frac{1}{\lambda} \left| \frac{V_{td}}{V_{cb}} \right|. \quad (11)$$

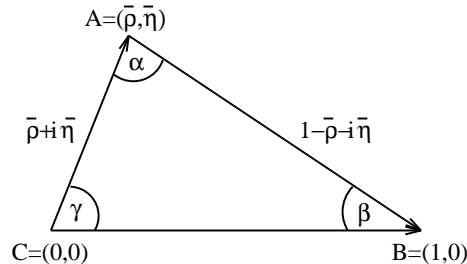


Figure 2: The Unitarity Triangle.

The angles β and $\gamma = \delta$ of the unitarity triangle are related directly to the complex phases of the CKM-elements V_{td} and V_{ub} , respectively, through

$$V_{td} = |V_{td}|e^{-i\beta}, \quad V_{ub} = |V_{ub}|e^{-i\gamma}. \quad (12)$$

Each of the angles is the relative phase of two adjacent sides (a part for possible extra π and minus sign) so that:

$$\beta = \arg\left(\frac{V_{td}V_{ub}^*}{V_{cd}V_{cb}^*}\right) = \text{atan}\left(\frac{\bar{\eta}}{1-\bar{\rho}}\right) \quad (13)$$

$$\gamma = \arg\left(\frac{V_{ud}V_{ub}^*}{V_{cd}V_{cb}^*}\right) = \text{atan}\left(\frac{\bar{\eta}}{\bar{\rho}}\right) \quad (14)$$

- The unitarity relation (Eq. 8) can be rewritten as

$$R_b e^{i\gamma} + R_t e^{-i\beta} = 1 \quad (15)$$

- The angle α can be obtained through the relation $\alpha + \beta + \gamma = 180^\circ$ expressing the unitarity of the CKM-matrix.

The triangle shown in Figure 2 -which depends on two parameters $(\bar{\rho}, \bar{\eta})$ -, plus $|V_{us}|$ and $|V_{cb}|$ give the full description of the CKM matrix.

The Standard Model, with three families of quarks and leptons, predicts that all measurements have to be consistent with the point $A(\bar{\rho}, \bar{\eta})$.

4.2 General Introduction to Oscillation and CP Violation

In this section we give a general introduction to the oscillation and CP violation formalism in view of their impact on the CKM matrix element determination.

A general system which satisfies the coupled Schrodinger equation can be written as:

$$i \frac{d}{dt} \begin{pmatrix} B^0 \\ \bar{B}^0 \end{pmatrix} = H \begin{pmatrix} B^0 \\ \bar{B}^0 \end{pmatrix} \quad (16)$$

$$H = \begin{pmatrix} H_{11} & H_{12} \\ H_{21} & H_{22} \end{pmatrix}; \quad H_{ij} = M_{ij} - i\Gamma_{ij}/2$$

The B^0 and the \bar{B}^0 are the flavour eigenstates. Transitions between B^0 and \bar{B}^0 are then possible and the Hamiltonian has to be diagonalized to find the new eigenstates which are:

$$|B_L^0\rangle = p|B^0\rangle + q|\bar{B}^0\rangle; \quad |B_H^0\rangle = p|B^0\rangle - q|\bar{B}^0\rangle \quad (17)$$

where $|q|^2 + |p|^2 = 1$. Solving the eigenvalues equation (supposing that CPT is conserved) and defining $\Delta m = M_H - M_L$ and $\Delta\Gamma = \Gamma_H - \Gamma_L$ it follows:

$$\Delta m^2 - 1/4\Delta\Gamma^2 = 4|M_{12}|^2 - |\Gamma_{12}|^2 \quad (18)$$

$$\Delta m\Delta\Gamma = 4\text{Re}(M_{12}\Gamma_{12}^*)$$

In the Standard Model, $B^0 - \bar{B}^0$ transitions occur through a second-order process -a box diagram- with a loop that contains W and up-type quarks. The exchange of the top quark dominates the part relative to the mass difference (M_{12}), while light quarks contribute to the part relative to the decay (Γ_{12}) (only common states to B^0 and \bar{B}^0 contribute). It results that : $\Gamma_{12}/M_{12} = m_b^2/m_t^2 \ll 1$. The relations (19) simplify to:

$$\Delta m = 2|M_{12}| \quad (19)$$

$$\Delta\Gamma = \frac{2\text{Re}(M_{12}\Gamma_{12}^*)}{|M_{12}|}$$

$$\frac{q}{p} = -\frac{|M_{12}|}{M_{12}}$$

The last expression is valid at leading approximation¹⁰. We are now interested in the time evolution

¹⁰Beyond the leading approximation the expression become : $\frac{q}{p} = -\frac{\Delta m - i/2\Delta\Gamma}{2M_{12} - i\Gamma_{12}}$

of the flavour eigenstates in the hypothesis ($\Delta\Gamma \ll \Delta m$):

$$\begin{aligned} |B_{phys.}^0(t)\rangle &= e^{-imt} e^{-\Gamma/2 t} (\cos \Delta m/2t |B^0\rangle + i \frac{q}{p} \sin \Delta m t/2 |\bar{B}^0\rangle) \\ |\bar{B}_{phys.}^0(t)\rangle &= e^{-imt} e^{-\Gamma/2t} (\cos \Delta m/2t |\bar{B}^0\rangle + i \frac{q}{p} \sin \Delta m t/2 |B^0\rangle) \end{aligned}$$

It follows:

$$\begin{aligned} \langle f|H|B_{phys.}^0(t)\rangle|^2 &= \tag{20} \\ &= \frac{e^{-\Gamma t}}{2} [(1 + \cos \Delta m t) |\langle f|H|B^0(t)\rangle|^2 + \\ &\quad (1 - \cos \Delta m t) |\frac{q}{p}|^2 |\langle f|H|\bar{B}^0(t)\rangle|^2 + \\ &\quad 2\text{Im} (|\frac{q}{p}| \sin \Delta m t \langle f|H|B^0(t)\rangle \langle f|H|\bar{B}^0(t)\rangle^*)] \end{aligned}$$

The probability that a meson B^0 produced (by strong interaction) at time $t = 0$ transforms (by weak interaction) into a \bar{B}^0 (or stays as a B^0) at time t is given by:

$$Prob(B_{phys.}^0(t) \rightarrow B_{phys.}^0(t) (\bar{B}_{phys.}^0(t))) = \frac{1}{2} e^{-\Gamma t} (1 + (-) \cos \Delta m t) \tag{21}$$

Defining:

$$\lambda = \frac{q \langle f|H|\bar{B}^0\rangle}{p \langle f|H|B^0\rangle} = \frac{q \bar{A}_f}{p A_f} ; \quad \bar{\lambda} = \frac{p \langle \bar{f}|H|B^0\rangle}{q \langle \bar{f}|H|\bar{B}^0\rangle} = \frac{p A_{\bar{f}}}{q \bar{A}_{\bar{f}}} \tag{22}$$

the equation becomes:

$$\begin{aligned} |\langle f|H|B_{phys.}^0(t)\rangle|^2 &= \tag{23} \\ &= \frac{e^{-\Gamma t}}{2} |\langle f|H|B^0(t)\rangle|^2 \\ &\quad [(1 + \cos \Delta m t) + \\ &\quad (1 - \cos \Delta m t) |\lambda|^2 \\ &\quad - 2\text{Im}(\lambda) \sin \Delta m t] \end{aligned}$$

and similarly for $|\langle f|H|\bar{B}_{phys.}^0(t)\rangle|$, $|\langle \bar{f}|H|B_{phys.}^0(t)\rangle|$ and $|\langle \bar{f}|H|\bar{B}_{phys.}^0(t)\rangle|$. We concentrate here on the two cases of CP violation which are the most relevant for CKM physics.

B⁰ sector: direct CP Violation and CP Violation in the interference between mixing and decays.

CP violation can occur because $\text{Im}\lambda \neq \text{Im}\bar{\lambda}$ and/or when $|\lambda|$, $|\bar{\lambda}|$ are different from unity. In this case the four quantities $Prob(B_{phys.}^0 \rightarrow f)$, $Prob(\bar{B}_{phys.}^0 \rightarrow f)$, $Prob(B_{phys.}^0 \rightarrow \bar{f})$ and $Prob(\bar{B}_{phys.}^0 \rightarrow \bar{f})$ (see eq. 24) have to be studied and thus $|\lambda|^2$, $|\bar{\lambda}|^2$, $\text{Im}\lambda$, $\text{Im}\bar{\lambda}$ are determined. The simplest case is when the final state f is a specific CP state. In this case $\bar{\lambda} = 1/\lambda \equiv \lambda_f$ and the previous conditions simplify to $\text{Im}\lambda_f \neq 0$ and/or $|\lambda_f| \neq 1$. The following asymmetry can be studied:

$$\begin{aligned} A_{CP}(\text{mixing} - \text{decay}) &= \frac{Prob(B_{phys.}^0(\Delta t) \rightarrow f) - Prob(\bar{B}_{phys.}^0(\Delta t) \rightarrow f)}{Prob(B_{phys.}^0(\Delta t) \rightarrow f) + Prob(\bar{B}_{phys.}^0(\Delta t) \rightarrow f)} \tag{24} \\ &= C_f \cos \Delta m_d \Delta t + S_f \sin \Delta m_d \Delta t , \end{aligned}$$

where

$$C_f = \frac{1 - |\lambda_f|^2}{1 + |\lambda_f|^2} ; \quad S_f = -\frac{2 \text{Im}\lambda_f}{1 + |\lambda_f|^2} \tag{25}$$

C_f corresponds to direct CP violation, since it is related to differences in the decay amplitudes, while S_f is related to the interference between the mixing and decays, involving the imaginary parts of p/q and

of the decay amplitudes. It is important to note that, also in case $|\lambda_f|=1$, CP violation is possible if $\text{Im}\lambda_f \neq 0$. This case is particularly interesting. When only one amplitude dominates the decay process, $|\lambda_f| = 1$, implying $C_f = 0$ and $S_f = -\text{Im}\lambda_f$. We will see in the following that $-\text{Im}\lambda_f$ is the sine of twice an angle of the unitarity triangle.

B⁺ sector: the direct CP Violation.

The transition amplitudes can be written as:

$$\begin{aligned} |\langle f|H|B^+ \rangle| &= v_1 A_1 e^{i\theta_1} + v_2 A_2 e^{i\theta_2} \\ |\langle \bar{f}|H|B^- \rangle| &= v_1^* A_1 e^{i\theta_1} + v_2^* A_2 e^{i\theta_2} \end{aligned} \quad (26)$$

where $v_{1,2}$ are the weak-CKM couplings and $A_{1,2}(\theta_{1,2})$ are the modulus and the strong phase respectively. The weak phase changes sign under CP (the strong phase do not). It follows:

$$\begin{aligned} a_{CP}(\text{direct}) &= \frac{|\langle f|H|B^+ \rangle|^2 - |\langle \bar{f}|H|B^- \rangle|^2}{|\langle f|H|B^+ \rangle|^2 + |\langle \bar{f}|H|B^- \rangle|^2} \\ &= \frac{2r_B \sin(\arg(v_1/v_2)) \sin(\theta_1 - \theta_2)}{1 + r_B^2 + 2r_B \cos(\arg(v_1/v_2)) \cos(\theta_1 - \theta_2)} \quad ; \quad r_B = \frac{|v_1|A_1}{|v_2|A_2} \end{aligned} \quad (27)$$

The basic conditions to have direct CP violation are the presence of two competing amplitudes, $r_B \neq 0$, and of nonzero weak phase and strong phase differences.

The weak phase difference is related to one of the unitarity triangle angles. To be more explicit, if for instance we consider a process which can occur through V_{ub} and V_{cb} mediated transitions, $\arg(v_1/v_2) = \gamma$.

CP Violation in the Kaon sector.

Historically the parameter characterizing CP violation was defined as ϵ given in:

$$|K_S \rangle = \frac{|K_1 \rangle + \epsilon K_2 \rangle}{\sqrt{1 + |\epsilon|^2}} \quad ; \quad |K_L \rangle = \frac{|K_2 \rangle + \epsilon K_1 \rangle}{\sqrt{1 + |\epsilon|^2}} \quad (28)$$

$K_{1,2}$ are the CP eigenstates and the previous equation can be written in terms of flavour eigenstates:

$$\begin{aligned} |K_S \rangle &= \frac{1}{\sqrt{2} \sqrt{1 + |\epsilon|^2}} [(1 + \epsilon)|K^0 \rangle + (1 - \epsilon)|\bar{K}^0 \rangle] \\ |K_L \rangle &= \frac{1}{\sqrt{2} \sqrt{1 + |\epsilon|^2}} [(1 + \epsilon)|K^0 \rangle - (1 - \epsilon)|\bar{K}^0 \rangle] \end{aligned}$$

where ϵ is related to p, q parameters by: $\epsilon = \frac{p-q}{p+q}$.

Two CP violating quantities are measured in the neutral Kaon sector:

$$\eta_{00} = \frac{\langle \pi^0 \pi^0 | H | K_L \rangle}{\langle \pi^0 \pi^0 | H | K_S \rangle} \quad ; \quad \eta_{\pm} = \frac{\langle \pi^+ \pi^- | H | K_L \rangle}{\langle \pi^+ \pi^- | H | K_S \rangle} \quad (29)$$

Defining

$$\begin{aligned} A_{00} &= \langle \pi^0 \pi^0 | H | K^0 \rangle \quad ; \quad \bar{A}_{00} = \langle \pi^0 \pi^0 | H | \bar{K}^0 \rangle \\ A_{+-} &= \langle \pi^+ \pi^- | H | K^0 \rangle \quad ; \quad \bar{A}_{+-} = \langle \pi^+ \pi^- | H | \bar{K}^0 \rangle \\ \lambda_{00} &= \frac{q \bar{A}_{00}}{p A_{00}} \quad ; \quad \lambda_{+-} = \frac{q \bar{A}_{+-}}{p A_{+-}} \end{aligned}$$

which implies

$$\eta_{00} = \frac{1 - \lambda_{00}}{1 + \lambda_{00}} \quad ; \quad \eta_{+-} = \frac{1 - \lambda_{+-}}{1 + \lambda_{+-}} \quad (30)$$

The $\pi\pi$ final states can have isospin $I=0,2$. Experimentally it is observed that $A_{I=2}/A_{I=0} \simeq 1/20$ (known has the $\Delta I=1/2$ rule). In the approximation that only the $I=0$ amplitude contributes -no direct CP violation- it follows:

$$\epsilon_K = \frac{\langle \pi^0 \pi_{I=0}^0 | H | K_L \rangle}{\langle \pi^0 \pi_{I=0}^0 | H | K_S \rangle} = \eta_{00} \quad (31)$$

and similarly for the η_{+-} .

Contrarily to B mesons, in case of Kaon physics $\Delta\Gamma \simeq \Delta M$. Using the expression of q/p (eq. 19) it follows that:

$$\epsilon_K = \frac{e^{i\pi/4}}{\sqrt{2}\Delta m_K} (\text{Im}M_{12} + 2\zeta\text{Re}M_{12}) \quad (32)$$

where $\zeta = \text{Im}(A(K \rightarrow \pi\pi)_{I=0})/\text{Re}(A(K \rightarrow \pi\pi)_{I=0})$. The contribution, proportional to ζ , which is of about 2% correction to $|\epsilon_K|$ can be neglected.

4.3 Standard Model formulae relating $\bar{\rho}$ and $\bar{\eta}$ to experimental and theoretical inputs

Five measurements restrict, at present, the possible range of variation of the $\bar{\rho}$ and $\bar{\eta}$ parameters:

- B hadrons can decay through the $b \rightarrow c$ and $b \rightarrow u$ transitions. Semileptonic decays offer a relatively large branching fraction ($\simeq 10\%$) and corresponding measurements can be interpreted using a well established theoretical framework. The relative rate of charmless over charmed b -hadron semileptonic decays is proportional to the square of the ratio:

$$\left| \frac{V_{ub}}{V_{cb}} \right| = \frac{\lambda}{1 - \frac{\lambda^2}{2}} \sqrt{\bar{\rho}^2 + \bar{\eta}^2}, \quad (33)$$

and it allows to measure the length of the side AC of the triangle (Figure 3).

- In the Standard Model, $B^0 - \bar{B}^0$ oscillations occur through a second-order process -a box diagram with a loop that contains W and up-type quarks. The box diagram with the exchange of a *top* quark gives the dominant contribution. The oscillation probability is given in eq. (21) and the time oscillation frequency, which can be related to the mass difference between the light and heavy mass eigenstates of the $B_d^0 - \bar{B}_d^0$ system (eq. 20, $\Delta m = 2|M_{12}|$), is expressed, in the SM, as¹¹:

$$\Delta m_d = \frac{G_F^2}{6\pi^2} m_W^2 \eta_b S(x_t) A^2 \lambda^6 [(1 - \bar{\rho})^2 + \bar{\eta}^2] m_{B_d} f_{B_d}^2 \hat{B}_{B_d}, \quad (34)$$

where $S(x_t)$ is the Inami-Lim function [26] and $x_t = m_t^2/M_W^2$, m_t is the \overline{MS} top quark mass, $m_t^{\overline{MS}}(m_t^{\overline{MS}})$, and η_b is the perturbative QCD short-distance NLO correction. The value of $\eta_b = 0.55 \pm 0.01$ has been obtained in [27] and $m_t = (167 \pm 5)$ GeV is used, as deduced from measurements by CDF and D0 Collaborations [21]. The remaining factor, $f_{B_d}^2 \hat{B}_{B_d}$, encodes the information of non-perturbative QCD. Apart for $\bar{\rho}$ and $\bar{\eta}$, the most uncertain parameter in this expression is $f_{B_d} \sqrt{\hat{B}_{B_d}}$ (6.4).

In the vacuum saturation approximation the matrix element of the V-A current is calculated between the vacuum and the pseudoscalar meson and only the axial current contributes. The constant f_{B_d} translates the probability that the quark and the antiquark meet to decay or the size of the B meson wave function at the origin. Another parameter is also introduced: the bag factor \hat{B}_{B_d} which is inserted to take into account all possible deviation from vacuum saturation approximation. The values of the bag factors are expected to be close of the unity.

The measurement of Δm_d gives a constraint on the length of the side AB of the triangle (Figure 3).

¹¹ Δm_q is usually expressed in ps^{-1} unit. 1 ps^{-1} corresponds to $6.58 \cdot 10^{-4} \text{ eV}$.

- The $B_s^0 - \overline{B}_s^0$ time oscillation frequency, which can be related to the mass difference between the light and heavy mass eigenstates of the $B_s^0 - \overline{B}_s^0$ system, is proportional to the square of the $|V_{ts}|$ element. Neglecting terms, having a small contribution, $|V_{ts}|$ is independent of $\overline{\rho}$ and $\overline{\eta}$. The measurement of Δm_s would then give a strong constraint on the non-perturbative QCD parameter $f_{B_s}^2 \hat{B}_{B_s}$. In any case, the ratio between the values of the mass difference between the mass-eigenstates, measured in the B_d^0 and in the B_s^0 systems can be used:

$$\frac{\Delta m_d}{\Delta m_s} = \frac{m_{B_d} f_{B_d}^2 \hat{B}_{B_d}}{m_{B_s} f_{B_s}^2 \hat{B}_{B_s}} \left(\frac{\lambda}{1 - \frac{\lambda^2}{2}} \right)^2 \frac{(1 - \overline{\rho})^2 + \overline{\eta}^2}{\left(1 + \frac{\lambda^2}{1 - \frac{\lambda^2}{2}} \overline{\rho} \right)^2 + \lambda^4 \overline{\eta}^2}. \quad (35)$$

The advantage in using the ratio $\frac{\Delta m_d}{\Delta m_s}$, instead of only Δm_d , is that the ratio $\xi = f_{B_s} \sqrt{\hat{B}_{B_s}} / f_{B_d} \sqrt{\hat{B}_{B_d}}$ is expected to be better determined from theory than the individual quantities entering into its expression. The measurement of the ratio $\Delta m_d / \Delta m_s$ gives a similar type of constraint as Δm_d , on the length of the side AB of the triangle.

- Indirect CP violation in the $K^0 - \overline{K}^0$ system is usually expressed in terms of the $|\varepsilon_K|$ parameter (as defined in Section 4.2) which is the fraction of CP violating component in the mass eigenstates. In the SM, the following equation is obtained

$$|\varepsilon_K| = C_\varepsilon A^2 \lambda^6 \overline{\eta} \times \left[-\eta_1 S(x_c) \left(1 - \frac{\lambda^2}{2} \right) + \eta_2 S(x_t) A^2 \lambda^4 (1 - \overline{\rho}) + \eta_3 S(x_c, x_t) \right] \hat{B}_K \quad (36)$$

where $C_\varepsilon = \frac{G_F^2 f_K^2 m_K m_W^2}{6\sqrt{2}\pi^2 \Delta m_K}$.

$S(x_i)$ and $S(x_i, x_j)$ are the appropriate Inami-Lim functions [26] depending on $x_q = m_q^2 / m_W^2$, including the next-to-leading order QCD corrections [27, 28]. The most uncertain parameter is \hat{B}_K (6.4).

The constraint brought by the measurement of $|\varepsilon_K|$ corresponds to an hyperbola in the $(\overline{\rho}, \overline{\eta})$ plane (Figure 3).

- The measurement of CP violation in the B sector.

The mixing induced CP asymmetry, $a_{J/\psi K_S}$, in $B_d^0 \rightarrow J/\psi K_S$ or $(\rightarrow J/\psi K_L)$ decays allows to determine the angle β of the Unitarity Triangle essentially without any hadronic uncertainties. As explained before, a possible manifestation of the CP asymmetry could appear in the interference between amplitudes describing decays with and without mixing. The process $B^0 \rightarrow J/\Psi K^0$ is dominated by tree diagram¹² and it follows that:

$$\begin{aligned} \frac{q}{p} &= \left(\frac{V_{tb}^* V_{td}}{V_{tb} V_{td}^*} \right) && \text{from B mixing} \\ \frac{\langle J/\Psi K^0 | H | \overline{B}^0 \rangle}{\langle J/\Psi K^0 | H | B^0 \rangle} &= \left(\frac{V_{cs}^* V_{cb}}{V_{cs} V_{cb}^*} \right) && \text{from B decay amplitudes} \\ &= \left(\frac{V_{cd}^* V_{cs}}{V_{cd} V_{cs}^*} \right) && \text{from K mixing} \\ |\lambda_f|^2 &= 1 && ; \quad \text{Im } \lambda_f = \eta_{CP} \sin 2\beta \end{aligned}$$

where η_{CP} is the CP eigenvalue of the final state. The asymmetry defined in eq. 25 gives:

$$A_{CP}(J/\Psi K_S) = -2 \sin(2\beta) \sin \Delta m_d \Delta t, \quad (37)$$

¹²The same process could be described by a Penguin diagram (with a ts transition) and a J/Ψ emitted from gluons. This process is proportional to $V_{ts} V_{tb}^*$. It is important to note that the amplitude associated to this process has the same phase, at order $\mathcal{O}(\lambda^2)$, as the dominant tree-level one. At order $\mathcal{O}(\lambda^4)$, V_{ts} is complex and differs from V_{cb} . Thus the correction to β is suppressed by a factor $\mathcal{O}(\lambda^4)$ and by an extra factor because the J/Ψ must be emitted by at least three gluons.

The measurement of $A_{CP}(J/\Psi K^0)$ gives a constraint corresponding to $\sin(2\beta)$, in the $(\bar{\rho}, \bar{\eta})$ plane (Figure 3).

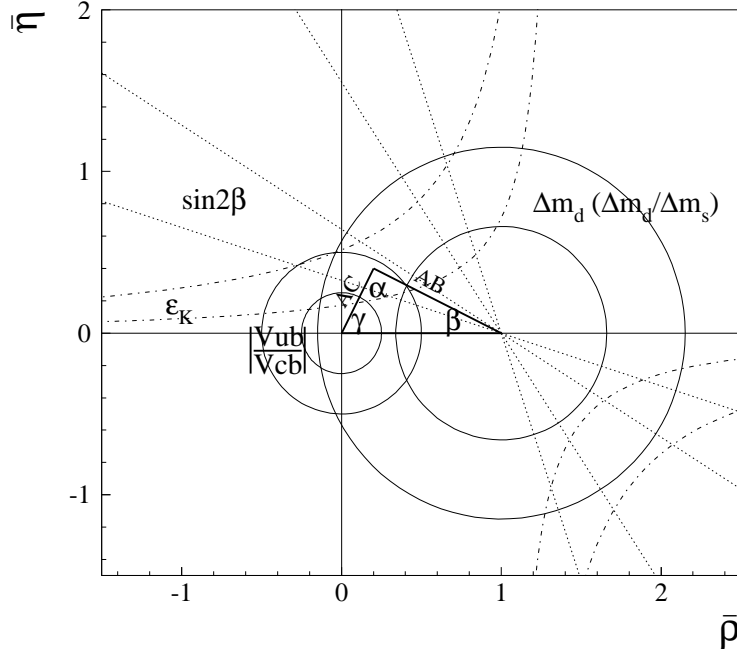


Figure 3: Unitarity Triangle. Constraints from $|V_{ub}|/|V_{cb}|$, $|\varepsilon_K|$, Δm_d or $\Delta m_d/\Delta m_s$ and $\sin(2\beta)$ are shown.

Constraints on $\bar{\rho}$ and $\bar{\eta}$ are obtained by comparing present measurements with theoretical expectations using the expressions given above and taking into account the different sources of uncertainties. In addition to $\bar{\rho}$ and $\bar{\eta}$, these expressions depend on other quantities. Additional measurements or theoretical determinations have been used to provide information on the values of these parameters; details are given in the next sections.

To illustrate the different constraints described in the present section, in Figure 3, the uncertainty bands for the quantities, obtained using Eqs. (33)–(37), are presented. Each band, corresponds to only one of the constraints and contains 95% of the events obtained by varying the input parameters.

In the first column of Table 2 the different measured quantities are listed, with their explicit dependence on $\bar{\rho}$ and $\bar{\eta}$ given in the third column.

Measurement	CKM×other	Constraint
$Br(b \rightarrow u\bar{\nu})/Br(b \rightarrow c\bar{\nu})$	$ V_{ub}/V_{cb} ^2$	$\bar{\rho}^2 + \bar{\eta}^2$
Δm_d	$ V_{td} ^2 f_{B_d}^2 B_{B_d} f(m_t)$	$(1 - \bar{\rho})^2 + \bar{\eta}^2$
$\frac{\Delta m_d}{\Delta m_s}$	$\left \frac{V_{td}}{V_{ts}} \right ^2 \frac{f_{B_d}^2 B_{B_d}}{f_{B_s}^2 B_{B_s}}$	$(1 - \bar{\rho})^2 + \bar{\eta}^2$
$ \varepsilon_K $	$f(A, \bar{\eta}, \bar{\rho}, B_K)$	$\propto \bar{\eta}(1 - \bar{\rho})$
$A_{CP}(J/\Psi K^0)$	$\sin(2\beta)$	$2\bar{\eta}\bar{\rho}/[(1 - \bar{\rho})^2 + \bar{\eta}^2]$

Table 2: Different measurements contributing in the determination of $\bar{\rho}$ and $\bar{\eta}$, with their functional dependences.

The values and errors of the relevant quantities used in the fit of the CKM parameters are summarized in Table 3.

For the extraction of the CKM parameters we use the Bayesian approach [37]. In these lectures we do not enter into any details related to the statistical method. Here we want just to explain the splitting

of the errors as given in Table 3. We take a Gaussian distribution ($\mathcal{G}(x - x_0)$) when the uncertainty is dominated by statistical effects, or when there are several contributions of similar importance to systematic errors, so that the central limit theorem applies. We take a uniform p.d.f. if the parameter value is believed to be (almost) certainly within a given interval, and the points inside this interval are considered as equally probable. The second model is used for theoretical uncertainties. $\mathcal{U}(x) = 1/2\sigma_{\text{theo}}$ for $x \in [x_0 - \sigma_{\text{theo}}, x_0 + \sigma_{\text{theo}}]$ and $\mathcal{U}(x) = 0$ elsewhere. The combined p.d.f. (\mathcal{P}) is obtained by convoluting the Gaussian p.d.f. (\mathcal{G}) with the uniform p.d.f. (\mathcal{U}): $\mathcal{P} = \mathcal{G} \otimes \mathcal{U}$. When several determinations of the same quantity are available the final p.d.f. in the Bayesian approach, is obtained by taking the product of individual p.d.f.s (and normalizing the obtained distribution to unity). For more details on statistical methods see [29].

Parameter	Value	Gaussian (σ)	Uniform (half-width)	Ref.
λ	0.2241	0.0036	-	[30]
$ V_{cb} (\text{excl.})$	42.1×10^{-3}	2.2×10^{-3}	-	Section 6.1
$ V_{cb} (\text{incl.})$	41.4×10^{-3}	0.7×10^{-3}	0.6×10^{-3}	Section 6.1
$ V_{ub} (\text{excl.})$	33.0×10^{-4}	2.4×10^{-4}	4.6×10^{-4}	Section 6.2
$ V_{ub} (\text{incl.})$	40.9×10^{-4}	4.6×10^{-4}	3.6×10^{-4}	Section 6.2
Δm_d	0.502 ps ⁻¹	0.007 ps ⁻¹	-	Section 6.3
Δm_s	> 14.5 ps ⁻¹ at 95% C.L.	sensitivity 18.3 ps ⁻¹	-	Section 6.3
m_t	167 GeV	5 GeV	-	[21]
$f_{B_d} \sqrt{\hat{B}_{B_d}}$	223 MeV	33 MeV	± 12 MeV	Section 6.4
$\xi = \frac{f_{B_s} \sqrt{\hat{B}_{B_s}}}{f_{B_d} \sqrt{\hat{B}_{B_d}}}$	1.24	0.04	± 0.06	Section 6.4
η_b	0.55	0.01	-	[27]
\bar{B}_K	0.86	0.06	0.14	Section 6.4
$ \varepsilon_K $	2.280×10^{-3}	0.019×10^{-3}	-	[23]
η_1	1.38	0.53	-	[28]
η_2	0.574	0.004	-	[27]
η_3	0.47	0.04	-	[28]
f_K	0.159 GeV	fixed	-	[23]
Δm_K	0.5301×10^{-2} ps ⁻¹	fixed	-	[23]
$\sin(2\beta)$	0.739	0.048	-	Section 6.5
m_b	4.21 GeV	0.08 GeV	-	Section 6.1
m_c	1.3 GeV	0.1 GeV	-	Section 6.1
α_s	0.119	0.03	-	[28]
G_F	1.16639×10^{-5} GeV ⁻²	fixed	-	[23]
m_W	80.23 GeV	fixed	-	[23]
$m_{B_d^0}$	5.2794 GeV	fixed	-	[23]
$m_{B_s^0}$	5.3696 GeV	fixed	-	[23]
m_K	0.493677 GeV	fixed	-	[23]

Table 3: Values of the relevant quantities used in the fit of the CKM parameters. In the third and fourth columns the Gaussian and the flat parts of the uncertainty are given (see text), respectively. The central values and errors are those adopted at the end of the ‘‘CKM Unitarity Triangle’’ Workshops ([29],[30]) and by HFAG [31] and are given and explained in the following sections (as indicated in the last column). The averages for the non perturbative QCD parameters are made by the CKM-LDG group [32]

5 B Physics at different facilities

In this chapter we will discuss B physics at different machines. The main contributors in B hadron studies are:

- the e^+e^- colliders
 - the symmetric-B factories operating at $\Upsilon(4S)$ (ARGUS/CRYSTAL BALL and CLEO/CUSB experiments running at DORIS and CESR, respectively, from 1979 to 2002)
 - the asymmetric-B factories operating at $\Upsilon(4S)$ (Belle at KEK and BaBar at PEP experiments running from 1999)
 - the Z^0 resonance experiments (the LEP collaborations which run from 1989 to 1995 and the SLD collaboration at SLC which run from 1989 to 1998).
- the $p\bar{p}$ collider
 - the TeVatron collider, operating at $\sqrt{s} = 1.8$ TeV - phase I (D0 and CDF experiment from 1987 to 2000). They are presently running with an improved luminosity at $\sqrt{s} \simeq 1.9$ TeV -phase II.

An overview of these experiments, operating at different facilities, is given in Table 4.

At the $\Upsilon(4S)$, pairs of B^\pm and B_d^0 (\bar{B}_d^0) mesons are produced on top of the hadronic background continuum from lighter $q\bar{q}$ pairs. The two B mesons are created simultaneously in a L=1 coherent state, such that before the first decay the final state contains a B and a \bar{B} ; at the time of the decay of the first B meson, the second one is in the opposite flavour eigenstate. The production cross section is about 1.2 nb. Because of the energy available, only B^\pm and B_d^0 mesons are emitted. In symmetric B-factories B particles are produced almost at rest while at the asymmetric factories they have a boost of $\beta\gamma = 0.56$ (0.44) (for BaBar (Belle)). It is important to note that, in both cases, the average B momentum in the $\Upsilon(4S)$ rest frame is of the order of about 350 MeV/c.

Considering that the B lifetime is of the order of 1.6 ps, the flight distance of a B hadron, defined as $L = \gamma\beta c\tau$ is, on average, at asymmetric B-factories, of the order of 250 μm . This distance is measurable and highlights the greatest advantage of asymmetric B-factories where time dependent analyses, necessary for CP violation studies, are possible.

The B decay products are the only tracks produced in the events, there is no accompanying additional hadron. As a consequence the energy taken by each B meson is equal to the half the total energy in the e^+e^- center-of-mass frame; this constraint is, for instance, very important in rejecting the non-B events. The decay products of the two B particles are spread isotropically over the space and such events can be distinguished from the continuum which are more jetty-like.

At the Z^0 resonance, B hadrons are produced from the coupling of the Z^0 to a $b\bar{b}$ quark pair. The production cross section is of ~ 6 nb, which is five times larger than at the $\Upsilon(4S)$. Hadronic events account for about 70 % of the total production rate; among these, the fraction of $b\bar{b}$ events is $\sim 22\%$ ¹³, which is rather similar to the one observed when running at the $\Upsilon(4S)$ energy (~ 25 %). B hadrons are thus copiously produced¹⁴. The produced $b\bar{b}$ pair picks up from the vacuum other quark-antiquarks pairs and hadronizes into B hadrons plus few other particles. Therefore, not only B^\pm and B_d^0 mesons are produced, but also B_s^0 mesons or b -baryons can be present in the final state. The b and \bar{b} quarks hadronize independently. b quarks fragment differently from light quarks, because of their high mass as compared with Λ_{QCD} . As a result, B hadrons carry, on average, about 70% of the available beam energy, whereas the rest of the energy is distributed among the other particles emitted in the fragmentation process. As a consequence, the two B hadrons fly in opposite directions and their decay products belong to jets situated in two different hemispheres.

¹³whereas the fraction of $c\bar{c}$ events is $\sim 17\%$.

¹⁴In the intermediate energy region (“continuum”) where the annihilation through one photon is dominant (V-coupling) the cross section scales with the energy available in the center of mass (squared), being of the order of 30 pb at 30 GeV and of about 10 pb at 60 GeV. In this energy range the fraction of $b\bar{b}$ events is $\sim 9\%$ whereas the fraction of $c\bar{c}$ events is $\sim 35\%$ (being the coupling proportional to the square of the electric charge).

The hard fragmentation and the long lifetime of the b quark make that the flight distance of a B hadron at the Z pole, defined as $L = \gamma\beta c\tau$, is on average of the order of 3 mm.

At $p\bar{p}$ colliders, the situation is rather different. Here b quarks are produced mainly through the gluon-gluon fusion process $gg \rightarrow b\bar{b}$. At the Fermilab Collider ($\sqrt{s} = 1.8$ TeV), the differential b -production cross section depends on the rapidity and on the transverse momentum. In total, it is typically of the order of $50\mu\text{b}$, which is large. B decay products are situated inside events having a average multiplicity which is much larger than the multiplicity at the Z pole. Furthermore the ratio $\sigma_{b\bar{b}}/\sigma_{tot}$ is of the order of a few per mill. As a consequence, only specific channels e.g. with fully reconstructed final states, or semileptonic decays, can be studied with a reasonable signal to background ratio.

Registered data sets from experiments operating at different facilities are summarized in Table 4.

Experiments	Number of $b\bar{b}$ events ($\times 1000000$)	Environment	Characteristics
LEP Coll.	~ 1 per expt. (4 expts.)	Z^0 decays ($\sigma_{b\bar{b}} \sim 6\text{nb}$)	back-to-back 45 GeV b-jets, all B hadron produced.
SLD	~ 0.1	Z^0 decays ($\sigma_{b\bar{b}} \sim 6\text{nb}$)	back-to-back 45 GeV b-jets, all B hadron produced, beam polarized.
ARGUS	~ 0.2	$\Upsilon(4S)$ decays ($\sigma_{b\bar{b}} \sim 1.2\text{nb}$)	mesons produced at rest, B_d^0 and B^+ .
CLEO	~ 9	$\Upsilon(4S)$ decays ($\sigma_{b\bar{b}} \sim 1.2\text{nb}$)	mesons produced at rest, B_d^0 and B^+ .
BaBar	~ 130	$\Upsilon(4S)$ decays ($\sigma_{b\bar{b}} \sim 1.2\text{nb}$)	asymmetric B-factories B_d^0 and B^+ .
Belle			
CDF	\sim several	$p\bar{p}$ collider-Run I $\sqrt{s} = 1.8$ TeV ($\sigma_{b\bar{b}} \sim 50\mu\text{b}$)	events triggered with leptons, all B hadron produced.

Table 4: Summary of recorded statistics by experiments operating at different facilities and main characteristics.

6 Evaluation of the parameters entering in the determination of the CKM parameters.

This section gives a short summary on the determination of the quantities entering in Unitarity Triangle fits. The discussion on the central values and attributed errors for these quantities has been extensively done and agreed values were adopted during the First Workshop on the ‘‘Unitarity Triangle Parameters Determination’’ held at CERN from the 12-15 February 2002 [29]. More recent values are taken from the updates done during the Second Workshop on the ‘‘Unitarity Triangle Parameters Determination’’ held at Durahm from the 5-9 April 2003 [30]. Many of the experimental averages have been calculated by the HFAG (Heavy Flavour Averaging Group) and can be found in [31].

6.1 Determination of $|V_{cb}|$

The $|V_{cb}|$ element of the CKM matrix can be accessed by studying the decay rate of inclusive and exclusive semileptonic b -decays.

6.1.1 Determination of $|V_{cb}|$ using inclusive analyses

The first method to extract $|V_{cb}|$ makes use of B-hadrons inclusive semileptonic decays and of the theoretical calculations done in the framework of the OPE (Operator Product Expansion). The inclusive

semileptonic width $\Gamma_{s.l.}$ is expressed as:

$$\Gamma_{s.l.} = \frac{BR(b \rightarrow cl\nu)}{\tau_b} = \gamma_{theory} |V_{cb}|^2;$$

$$\gamma_{theory} = f(\alpha_s, m_b, \mu_\pi^2, 1/m_b^3 \dots). \quad (38)$$

From the experimental point of view the semileptonic width has been measured by the LEP/SLD and $\Upsilon(4S)$ experiments with a relative precision of about 2%:

$$\begin{aligned} \Gamma_{sl} &= (0.431 \pm 0.008 \pm 0.007) 10^{-10} MeV & \Upsilon(4S) \\ \Gamma_{sl} &= (0.439 \pm 0.010 \pm 0.007) 10^{-10} MeV & \text{LEP/SLD} \\ \Gamma_{sl} &= (0.434 \times (1 \pm 0.018)) 10^{-10} MeV & \text{average} \end{aligned} \quad (39)$$

Using the theoretical determinations of the parameters entering into the expression of γ_{theory} in Eq. (38), the uncertainty on $|V_{cb}|$ comes out to be of the order of 5% ($2.0 \cdot 10^{-3}$). Thus the precision on the determination of $|V_{cb}|$ is limited by theoretical uncertainties which are mainly related to the non perturbative QCD parameters.

These parameters can be experimentally determined using the fact that OPE gives expressions in terms of operators whose averaged values are universal when considering different aspects of the same reaction.

Moments of the hadronic mass spectrum, of the lepton energy spectrum and of the photon energy in the $b \rightarrow s\gamma$ decay are sensitive to the same non perturbative QCD parameters contained in the factor γ_{theory} of Eq. (38) and, in particular, to the mass of the b and c quarks and to the Fermi motion of the heavy quark inside the hadron, μ_π^2 ¹⁵. For more details, see for instance [34],[35].

First measurements have been done by CLEO and preliminary results have been obtained by BaBar and DELPHI.

As an example, DELPHI data have been used for the determination of these non perturbative QCD parameters and an illustration of the obtained results is given in Figure 4.

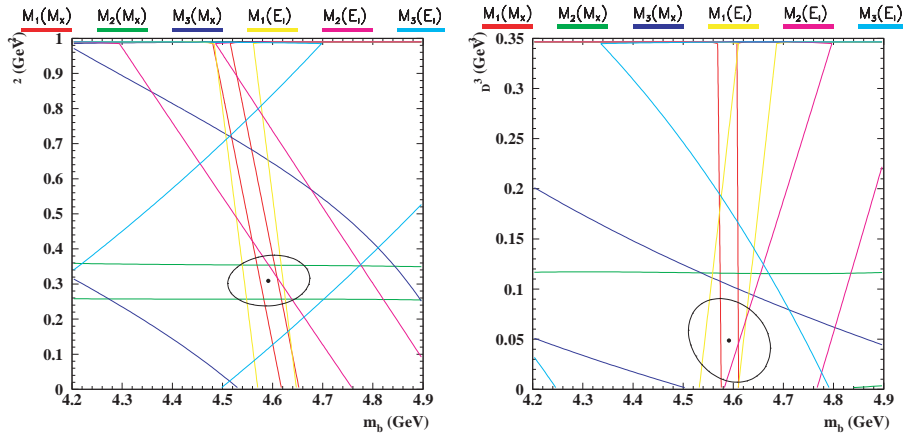


Figure 4: The moments analysis performed by DELPHI Collaboration [34]. The projection of the constraints, brought by six measured moments, over the $m_b - \mu_\pi^2$ (left) and $m_b - \rho_D^3$ (right) planes (ρ_D being related to the corrections corresponding to $1/m_b^3$ terms). The bands correspond to the total measurement accuracy and are given by keeping all other parameters fixed at their central values. The ellipses represent the 1σ contour.

Using the experimental results on Γ_{sl} , Eq. (39), and on the determination of the non perturbative QCD parameters, the following value for $|V_{cb}|$ is obtained:

$$|V_{cb}| = (41.4 \pm 0.7 \pm 0.6_{\text{theo.}}) 10^{-3} (\text{inclusive}) \quad (40)$$

¹⁵In another formalism, based on pole quark masses, the $\bar{\Lambda}$ and λ_1 parameters are used, which can be related to the difference between hadron and quark masses and to μ_π^2 , respectively.

This result brings an important improvement in the determination of the $|V_{cb}|$ element. The dominant part of the initial theoretical errors is now accounted for as experimental uncertainties, using the fitted non perturbative quantities (m_b , m_c , μ_π^2 and $1/m_b^3$ contributions) and the remaining theoretical error has been reduced by more than a factor three (previously the quoted theoretical error was $\pm 2.0 \cdot 10^{-3}$).

6.1.2 Determination of $|V_{cb}|$ using $B \rightarrow D^* \ell \nu$ analyses

An alternative method to determine $|V_{cb}|$ is based on exclusive $\overline{B}_d^0 \rightarrow D^{*+} \ell^- \overline{\nu}_\ell$ decays. Using HQET (Heavy Quark Effective Theory), an expression for the differential decay rate can be derived:

$$\frac{d\Gamma}{dw} = \frac{G_F^2}{48\pi^2} |V_{cb}^2| |F(w)|^2 G(w) ; w = v_B \cdot v_D \quad (41)$$

w is the 4-product of the B (v_B) and the D meson (v_D) velocities. $G(w)$ is a kinematical factor and $F(w)$ is the form factor describing the transition. At zero recoil ($w=1$) and for infinite quark masses, $F(1)$ goes to unity. The strategy is then to measure $d\Gamma/dw$, to extrapolate at zero recoil and to determine $F(1) \times |V_{cb}|$.

The world average result (as given in PDG 2004) [31] is:

$$|V_{cb}| = (42.1 \pm 1.1 \pm 1.9_{F(1)}) \cdot 10^{-3} = (42.1 \pm 2.2) \cdot 10^{-3} \quad (\text{exclusive}) \quad (42)$$

To evaluate $|V_{cb}|$, the value of $F(1) = 0.91 \pm 0.04$ have been used [39, 40].

6.1.3 Determination of $|V_{cb}|$ using inclusive and exclusive methods

Combining these two determinations of $|V_{cb}|$ gives:

$$|V_{cb}| = (41.5 \pm 0.8) \cdot 10^{-3} \quad (\text{exclusive} + \text{inclusive}) \quad (43)$$

The average has been obtained neglecting possible correlations between the two methods to determine of $|V_{cb}|$. This assumption is safe from the experimental point of view, whereas detailed studies are still missing from theory side. It should be noted that the inclusive method is dominating the final precision on $|V_{cb}|$.

To conclude, it is important to remind that, as $|V_{cb}| = A\lambda^2$, the measurement of $|V_{cb}|$ allows the determination of A one of the four free parameters of the CKM matrix. Furthermore $|V_{cb}|$ gives the scale of the Unitarity Triangle.

It is important to note also that $|V_{cb}|$, today, is known with 2% accuracy. This achievement has to be considered as a legacy from LEP and CLEO experiments.

6.2 Determination of $|V_{ub}|$

The measurement of $|V_{ub}|$ is rather difficult because one has to suppress the large background coming from the more abundant semileptonic b to c quark transitions.

Several new determinations of the CKM element $|V_{ub}|$ are now available [31]

6.2.1 Determination of $|V_{ub}|$ using inclusive analyses

As for $|V_{cb}|$, the extraction of $|V_{ub}|$ from inclusive semileptonic decays is based on HQET implemented through OPE.

By using kinematical and topological variables, it is possible to select samples enriched in $b \rightarrow u \ell^- \overline{\nu}_\ell$ transitions. There are, schematically, three main regions in the semileptonic decay phase space to be considered:

- the lepton energy end-point region: $E_\ell > \frac{M_B^2 - M_D^2}{2M_B}$ (which was at the origin for the first evidence of $b \rightarrow u$ transitions)
- the low hadronic mass region: $M_X < M_D$ (pioneered by the DELPHI Coll. [41])

- the high q^2 region: $M_{\ell\nu}^2 = q^2 > (M_B - M_D)^2$.

in which the background from $b \rightarrow c\ell^-\bar{\nu}_\ell$ decays is small.

A summary of the different determinations of $|V_{ub}|$ is given in Figure 5. For the extraction of the CKM parameters we use the average calculated in [29], presented in [41] and given in Table 3 :

$$|V_{ub}| = (40.9 \pm 4.6 \pm 3.6) \times 10^{-4} \quad \text{LEP-CLEO (inclusive)} \quad (44)$$

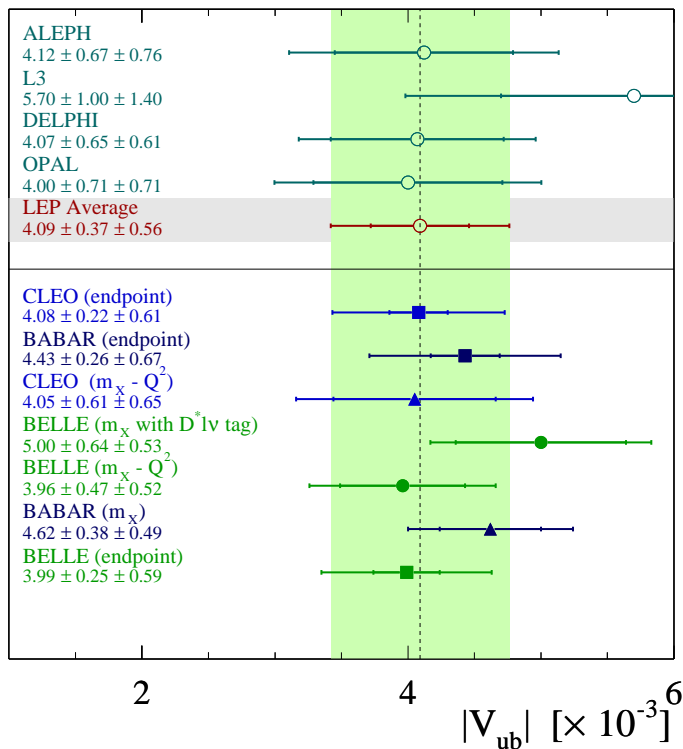


Figure 5: Summary of $|V_{ub}|$ inclusive measurements [31]. For the extraction of the CKM parameters we use the average calculated in [29], presented in [41] and given in Table 3.

6.2.2 Determination of $|V_{ub}|$ using exclusive analyses

The second method to determine $|V_{ub}|$ consists in the reconstruction of charmless semileptonic B decays: $\bar{B} \rightarrow \pi(\rho)\ell\bar{\nu}$.

Experimentally, the use of exclusive final states provides extra kinematical constraints for background suppression. Theoretically, the uncertainties are of a different nature as those already described in the inclusive analysis. The probability that the final state quarks form a given meson is described by form factors and, to extract $|V_{ub}|$ from actual measurements, the main problem rests in the determination of these hadronic form factors. As there is no heavy quark in the final state, symmetry arguments which were helpful to determine the form factor in $\bar{B} \rightarrow D^*\ell\bar{\nu}$ decays cannot be invoked. Light-Cone Sum Rules can provide an evaluation at the 15-20% accuracy level. Lattice QCD calculations give a similar precision but these uncertainties are expected to be reduced in the near future. The main limitation in lattice calculations is that, at present, they can be used only in the high q^2 region.

A summary of the different determinations of $|V_{ub}|$ can be found in [29] and [30]. The combined value of $|V_{ub}|$ is obtained by assuming that systematic uncertainties, attached to individual measurements, can be composed quadratically, for their uncorrelated components, and have correlated contributions,

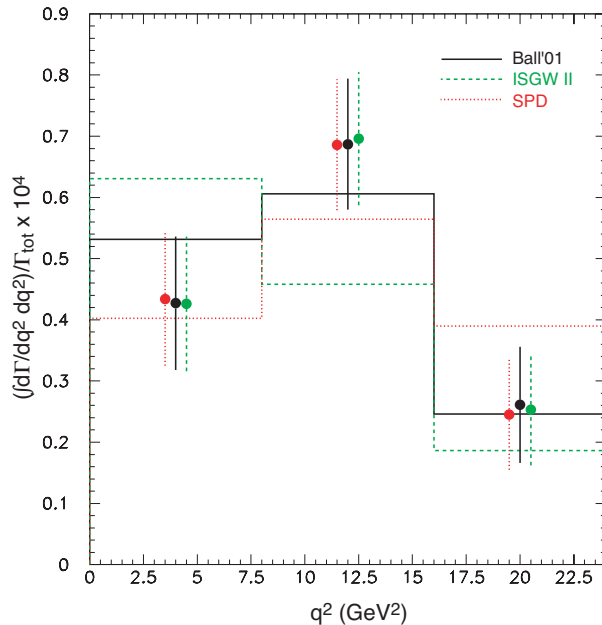


Figure 6: Differential branching fraction for $B^0 \rightarrow \pi^- \ell^+ \nu$ measured as a function of q^2 , by the CLEO Coll., and compared with predicted values (histograms) for three models used to extract $|V_{ub}|$.

of similar size. This correlated part of the systematics arises mainly from the modelling of the $b \rightarrow u$ background. The relative theoretical error is similar for all measurements and, for the time being, the error from the BaBar measurement is used. The result is

$$\begin{aligned}
 |V_{ub}| &= (33.8 \pm 2.4^{+3.7}_{-5.4}) \times 10^{-4} \\
 &= (33.0 \pm 2.4 \pm 4.6) \times 10^{-4}
 \end{aligned}
 \tag{45}$$

The accuracy on the determination of $|V_{ub}|$ using exclusive decays is limited by the theoretical uncertainty on hadronic form factor determination. An interesting analysis has been presented by the CLEO Collaboration at ICHEP02 [41], using the $B_d^0 \rightarrow \pi^- \ell^+ \nu_\ell$ decay mode, which consists in extracting the signal rates in three independent regions of q^2 . In this way it is possible to discriminate between models. The fit shows that the ISGW II model is compatible with data at only 1% probability level. This approach could be used, in future, to reduce the importance of theoretical errors, considering that the ISGW II gave, at present, the further apart V_{ub} determination [41].

6.2.3 Determination of $|V_{ub}|$ using inclusive and exclusive methods

Combining the two determinations of $|V_{ub}|$ (44,46), we obtain, in practice, almost a Gaussian p.d.f. corresponding to:

$$|V_{ub}| = (35.7 \pm 3.1) \times 10^{-4}. \tag{46}$$

New and more precise results from Belle and Babar Collaborations will much improve the present situation.

6.3 Measurements of $B^0 - \bar{B}^0$ oscillations

6.3.1 Measurements of the $B_d^0 - \bar{B}_d^0$ oscillation frequency: Δm_d

The probability that a B^0 meson oscillates into a \bar{B}^0 or remains as a B^0 is given in Eq. 21.

The measurement of Δm_d has been the subject of an intense experimental activity during the last ten years. Results are available which correspond to the combination of 27 analyses, using different event samples, performed by the LEP Coll./SLC/CDF/B-Factories experiments.

A typical proper time distribution is shown in Figure 8. The oscillating behaviour is clearly visible. Figure 7 gives the results for Δm_d , obtained by each experiment and the overall average [31]:

$$\Delta m_d = (0.502 \pm 0.007) \text{ ps}^{-1}. \quad (47)$$

The accuracy is of about 1%. The B-factories have the main contribution to this accuracy. Improvements can still be expected from these facilities and they are expected to reach a few per mill precision.

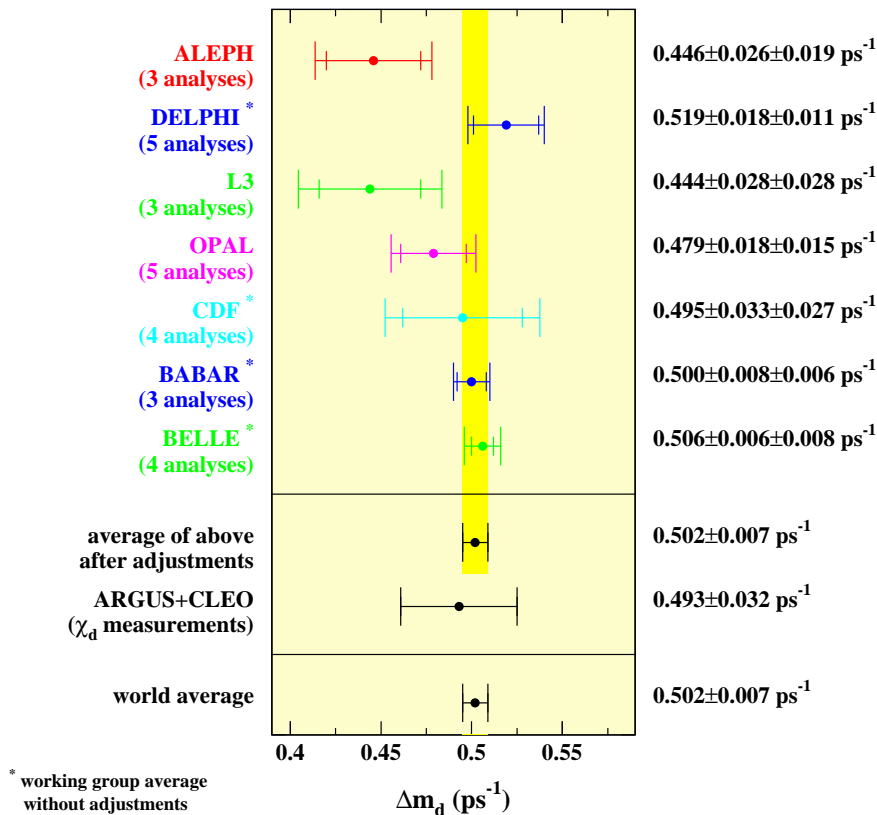


Figure 7: Summary of Δm_d measurements [31].

6.3.2 Search for $B_s^0 - \overline{B}_s^0$ oscillations

As the B_s^0 meson is expected to oscillate more than 20 times faster than the B_d^0 ($\Delta m_s/\Delta m_d \propto 1/\lambda^2$) and as B_s^0 mesons are less abundantly produced, the search for $B_s^0 - \overline{B}_s^0$ oscillations is more difficult. The observation of fast oscillations requires the highest resolution on the proper time and thus on the B_s^0 decay length.

No signal for $B_s^0 - \overline{B}_s^0$ oscillations has been observed so far.

The method used to measure or to put a limit on Δm_s consists in modifying Eq. (21) in the following way [42]:

$$1 \pm \cos(\Delta m_s t) \rightarrow 1 \pm \mathcal{A} \cos(\Delta m_s t). \quad (48)$$

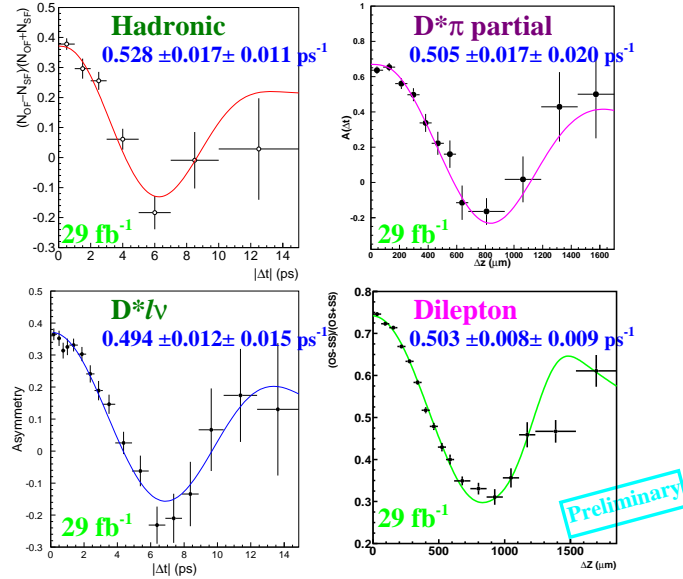


Figure 8: The plots show the $B_d^0 - \bar{B}_d^0$ oscillations (Belle Coll.). The points with error bars are the data. The result of the fit gives the value for Δm_d .

\mathcal{A} and its error, $\sigma_{\mathcal{A}}$, are measured at fixed values of Δm_s , instead of Δm_s itself. In case of a clear oscillation signal, at a given frequency, the amplitude should be compatible with $\mathcal{A} = 1$ at this frequency. With this method it is easy to set a limit. The values of Δm_s excluded at 95% C.L. are those satisfying the condition $\mathcal{A}(\Delta m_s) + 1.645 \sigma_{\mathcal{A}(\Delta m_s)} < 1$.

With this method, it is easy also to combine results from different experiments and to treat systematic uncertainties in the usual way since, for each value of Δm_s , a value for \mathcal{A} with a Gaussian error $\sigma_{\mathcal{A}}$, is measured. Furthermore, the sensitivity of a given analysis can be defined as the value of Δm_s corresponding to $1.645 \sigma_{\mathcal{A}(\Delta m_s)} = 1$ (using $\mathcal{A}(\Delta m_s) = 0$), namely supposing that the “true” value of Δm_s is well above the measurable value.

During last years, impressive improvements in the analysis techniques allowed to increase the sensitivity of the search for $B_s^0 - \bar{B}_s^0$ oscillations. Figure 9 gives details of the different Δm_s analyses. The combined result of LEP/SLD/CDF analyses [31] (Figure 10) corresponds to:

$$\Delta m_s > 14.5 \text{ ps}^{-1} \text{ at } 95\% \text{ C.L.}$$

with a sensitivity : $\Delta m_s = 18.3 \text{ ps}^{-1}$. (49)

The present combined limit implies that B_s^0 oscillate at least 30 times faster than B_d^0 mesons. Taking into account only the λ dependence of the ratio $\Delta m_d / \Delta m_s$ (eq. 35), this factor would be about 20. The present limit gives strong constraints on the $\bar{\rho}$ parameter whose value ends up to be about 0.2.

The significance of the “bump” appearing around 17 ps^{-1} is about 2.2σ and no claim can be made for the observation of $B_s^0 - \bar{B}_s^0$ oscillations.

Tevatron experiments are expected to measure soon these oscillations.

6.4 Some theoretical inputs: B_K , $f_B \sqrt{\hat{B}_B}$ and ξ

Constraints on $\bar{\rho}$ and $\bar{\eta}$ depend also upon three parameters which are related to the strong interaction operating in the non-perturbative regime: $f_B \sqrt{\hat{B}_B}$, ξ and B_K .

Expressions for these constraints have been given, respectively, in Eqs. (34), (35) and (37). Important improvements have been achieved during the last few years in the evaluation of these parameters in the framework of Lattice QCD and a world-wide effort is organized in view of having precise determinations

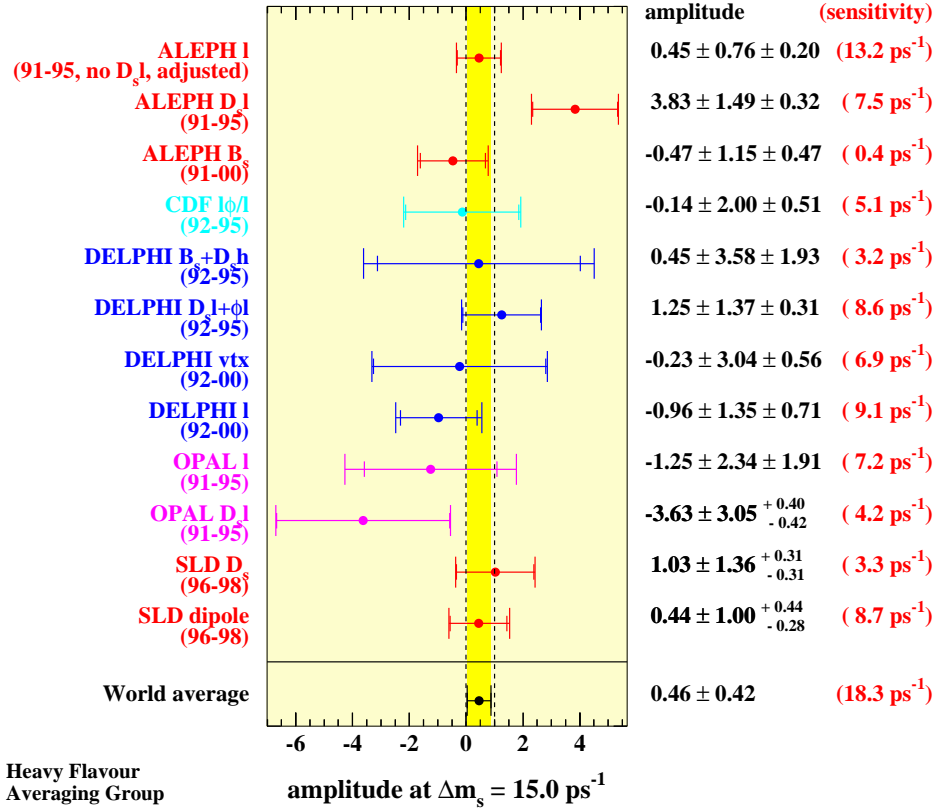


Figure 9: B_s^0 oscillation results. Values of the fitted amplitude at $\Delta m_s = 15 \text{ ps}^{-1}$ and of the sensitivity obtained by each experiment [31].

of these parameters. As a consequence, in this phenomenological analysis, only most recent results from Lattice QCD are used.

6.4.1 Brief introduction to Lattice QCD (LQCD)

Lattice QCD (LQCD) was invented about 25 years ago by K. Wilson [43].

Perturbation theory can be seen as a tool to perform functional integrals by which all vacuum expectation values of the quantum fields can be expressed. LQCD approach consists in a numerical evaluation of the functional integrals. It needs a discretization of the four-dimensional space-time by introducing a basic length, the lattice spacing (often indicated as a). So LQCD does not introduce new parameters or field variables in the discretization and it retains the same properties as QCD. In this sense, it is correct to say, that LQCD is not a model, as quark models for example, and therefore physical quantities can be computed from first principles without arbitrary assumptions. The only input parameters are the strong coupling constant and the six quark current masses.

Statistical errors.

Considering N points in each direction, the lattice will have a volume $(N a)^4$ (having so two natural cutoffs: a finite space resolution and a finite volume). The standard integrals are sampled over a finite net of points, whereas the functional integrals are sampled over a finite set of functions (or configurations). The vacuum expectation values are obtained by “averaging” over all the configurations. Those evaluations

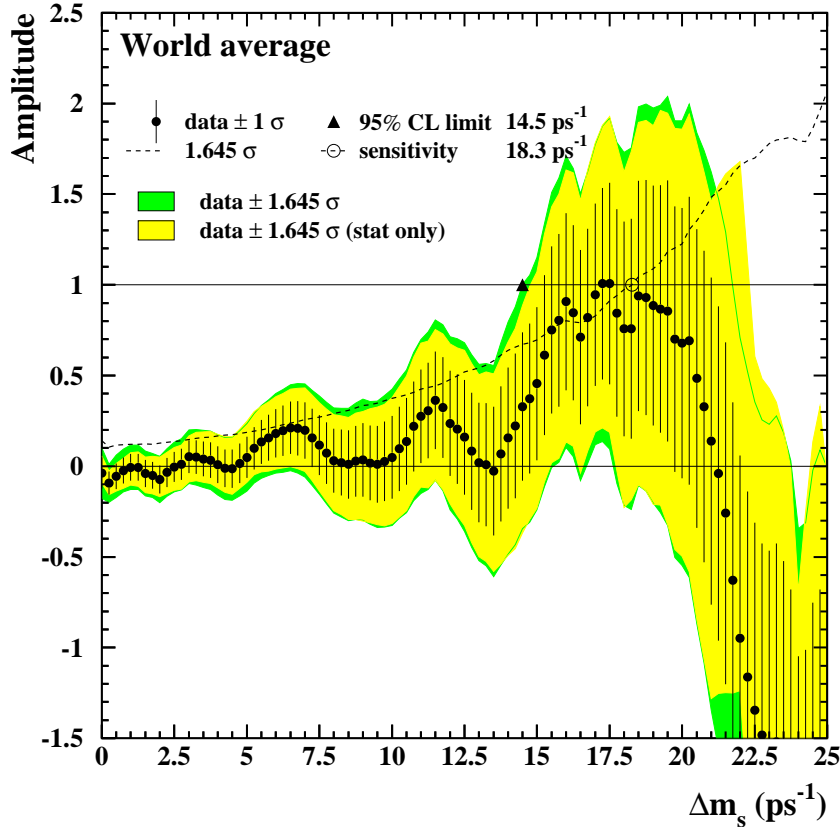


Figure 10: The plot [31] gives combined Δm_s results from LEP/SLD/CDF analyses shown as an amplitude versus Δm_s plot. The points with error bars are the data; the lines show the 95% C.L. curves (darker regions correspond to the inclusion of systematics). The dotted curve corresponds to the sensitivity.

are done using MonteCarlo techniques. In this spirit, LQCD simulations are theoretical experiments carried out by numerical integration of the functional integral by MonteCarlo techniques. In this respect uncertainties on output quantities are evaluated following criteria which are very close to those used in experimental measurements. Results are obtained with “statistical errors”, i.e. uncertainties originated by stochastic fluctuations, which may be reduced by increasing the sample of gluon-field configurations on which averages are performed. It is very reasonable to assume that the statistical fluctuations have a Gaussian distribution.

For several quantities statistical errors have been reduced to the percent level (or even less). However most of the results are affected by systematic effects.

Systematic errors.

Systematic uncertainties come from discretization effects, finite volume effects, the treatment of heavy quarks, chiral extrapolation and quenching. Errors coming from the discretization and from the finite volume can be addressed by brute-force improvements of numerical simulations or by improvements in the discretization procedures.

The quenched approximation is obtained by turning off virtual quark loops. An important consequence of this approximation is that the potential between a quark/antiquark pair depends on this approximation. In the full theory, at large distance, there is a screened potential between two hadrons because the string

breaks by the creation of a $q\bar{q}$ pair. In quenched LQCD the string does not couple to such pairs and the long distance behaviour of the two theories is rather different. This problem is not so important since, for the long distance scale which matters in hadronic physics, and in which we are interested, there is a “natural” cutoff of about one Fermi due to confinement.

It is reasonable to expect that quenching corrections are lying between 10-20% for most of evaluated physical quantities.

Because of computing limitations, most numbers have been obtained in the quenched approximation. Theoretical estimates and some preliminary results in the (partially) unquenched case are also available and are used to estimate the corresponding systematic error of quenched results.

These calculations are usually performed with two light quarks in the fermion loops, at values of the light-quark masses larger than the physical values and an extrapolation in these masses is required. Calculations are generally made at few values of the lattice spacing and thus contain discretization errors. An estimate of quenching errors is obtained by comparing quenched and unquenched results at similar values of the lattice spacing.

Another important issue is related to the chiral extrapolation. In fact it is difficult to simulate realistically light quarks, with their physical masses, and calculations are usually made for a set of (valence) quark masses, ranging from about $m_s/2$ to $2 m_s$. The results need then to be interpolated or extrapolated. Similar extrapolation needs to be done, in partially quenched calculations, considering the range of sea quark masses used. The problem arises since there are logarithmic dependences in physical quantities as the valence and/or the sea quark mass are extrapolated to their physical values (divergences in some cases if masses vanish). In practice different extrapolations can be performed if one considers or not these terms. The JLQCD collaboration finds [44] that these different extrapolations tend to decrease the value of f_{B_d} relative to f_{B_s} . At present a reasonable view [45, 39] is to allow a decrease of f_{B_d} by -10% and a negligible change in f_{B_s} .

For the present phenomenological analysis, the following values and errors have been used

$$\begin{aligned}
 f_{B_d} \sqrt{\hat{B}_{B_d}} &= (223 \pm 33 \pm 12) \text{ MeV} \\
 \xi &= \frac{f_{B_s} \sqrt{\hat{B}_{B_s}}}{f_{B_d} \sqrt{\hat{B}_{B_d}}} = 1.18 \pm 0.04 \pm 0.06 \\
 \hat{B}_K &= 0.86 \pm 0.06 \pm 0.14
 \end{aligned}
 \tag{50}$$

These estimates have to be considered as conservative, since they assume a maximal effect due to chiral extrapolation, reflected in the last error. These last errors are taken as flat distributions.

A detailed description on how these values have been obtained can be found in [29]. The CKM-LDG Group [32] is taking care of these averages.

6.5 Determination of $\sin(2\beta)$ from CP asymmetry in $J/\psi K^0$ decays.

BaBar and Belle collaborations have recently updated their measurements. The world average is [31]:

$$\sin(2\beta) = 0.739 \pm 0.048
 \tag{51}$$

All details concerning the analyses techniques are described in these proceeding by the seminar corresponding to U. Mallik.

7 Determination of the Unitarity Triangle parameters

In this section we give the results for the quantities defining the Unitarity Triangle, assuming the validity of the Standard Model: $\bar{\rho}$, $\bar{\eta}$, $\sin(2\beta)$, $\sin(2\alpha)$ and γ as well as for other quantities as Δm_s , f_B and \hat{B}_K . The inputs used are summarised in Table 3 (see Section 4.3).

For more details and concerning latest results see [46].

7.1 Fundamental test of the Standard Model in the fermion sector

The most crucial test consists in the comparison between the region selected by the measurements which are sensitive only to the sides of the Unitarity Triangle (semileptonic B decays and $B^0 - \bar{B}^0$ oscillations) and the regions selected by the direct measurements of CP violation in the kaon ($|\varepsilon_K|$) or in the B ($\sin(2\beta)$) sectors. This test is shown in Figure 11. It can be translated quantitatively through the comparison between the values of $\sin(2\beta)$ obtained from the measurement of the CP asymmetry in $J/\psi K^0$ decays and the one determined from “sides“ measurements:

$$\begin{aligned} \sin(2\beta) &= 0.685 \pm 0.047 [0.547 - 0.770] \text{ at } 95\% \text{ C.L.} && \text{sides only} \\ \sin(2\beta) &= 0.739 \pm 0.048 [0.681 - 0.787] \text{ at } 95\% \text{ C.L.} && J/\psi K^0. \end{aligned} \quad (52)$$

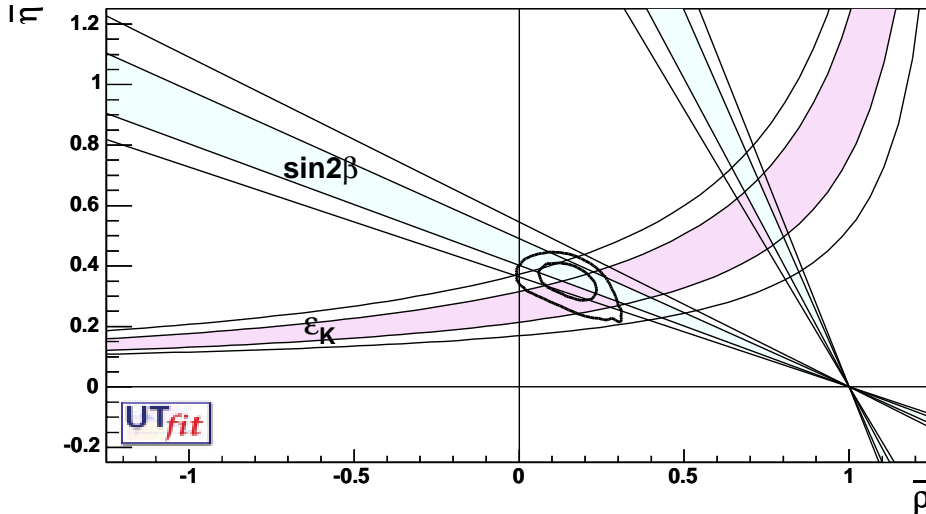


Figure 11: The allowed regions for $\bar{\rho}$ and $\bar{\eta}$ (contours at 68%, 95%) as selected by the measurements of $|V_{ub}|/|V_{cb}|$, ΔM_d , and by the limit on $\Delta M_s/\Delta M_d$ are compared with the bands (at 68% and 95% C.L.) from the measurements of CP violating quantities in the kaon ($|\varepsilon_K|$) and in the B ($\sin(2\beta)$) sectors.

The spectacular agreement between these values illustrates the consistency of the Standard Model in describing CP violation phenomenon in terms of one single parameter $\bar{\eta}$. It is also an important test of the OPE, HQET and LQCD theories which have been used to extract the CKM parameters.

It has to be noted that this test is significant provided the errors on $\sin(2\beta)$ from the two determinations are comparable.

Corresponding results, for the unitarity triangle parameters, are given in Table 5.

Parameter	68%	95%	99%
$\bar{\eta}$	$0.346^{+0.039}_{-0.043}$	(0.227-0.416)	(0.099-0.437)
$\bar{\rho}$	0.153 ± 0.061	(0.030-0.325)	(-0.012-0.368)
$\sin(2\beta)$	0.685 ± 0.047	(0.547-0.770)	(0.280-0.806)
$\sin(2\alpha)$	-0.01 ± 0.35	(-0.85-0.83)	-
$\gamma[^\circ]$	65.3 ± 9.5	(38.9-84.8)	(15.8-90.0)

Table 5: Values and probability ranges for the unitarity triangle parameters when the constraints from $|\varepsilon_K|$ and $\sin(2\beta)$ measurements are not used.

7.2 Determination of the Unitarity Triangle parameters : $\bar{\eta}$, $\bar{\rho}$, $\sin(2\beta)$, $\sin(2\alpha)$, γ

By using all five available constraints ($|V_{ub}|/|V_{cb}|$, Δm_d , $\Delta m_s/\Delta m_d$, $|\varepsilon_K|$ and $\sin(2\beta)$), the results given in Table 6 are obtained.

Parameter	68%	95%	99%
$\bar{\eta}$	0.342 ± 0.026	(0.291-0.396)	(0.272-0.415)
$\bar{\rho}$	0.174 ± 0.047	(0.076-0.260)	(0.045-0.293)
$\sin(2\beta)$	0.697 ± 0.035	(0.637-0.761)	(0.619-0.781)
$\sin(2\alpha)$	-0.15 ± 0.25	(-0.62-0.34)	(-0.73-0.50)
$\gamma[^\circ]$	61.1 ± 7.8	(48.6-76.0)	(43.2-82.9)

Table 6: Values and probability ranges for the unitarity triangle parameters obtained by using all five available constraints: $|V_{ub}|/|V_{cb}|$, Δm_d , $\Delta m_s/\Delta m_d$, $|\varepsilon_K|$ and $\sin(2\beta)$.

Figures 12 and 13 show, respectively, the corresponding selected region in the $(\bar{\rho}, \bar{\eta})$ plane and the p.d.f. for the Unitarity Triangle parameters.

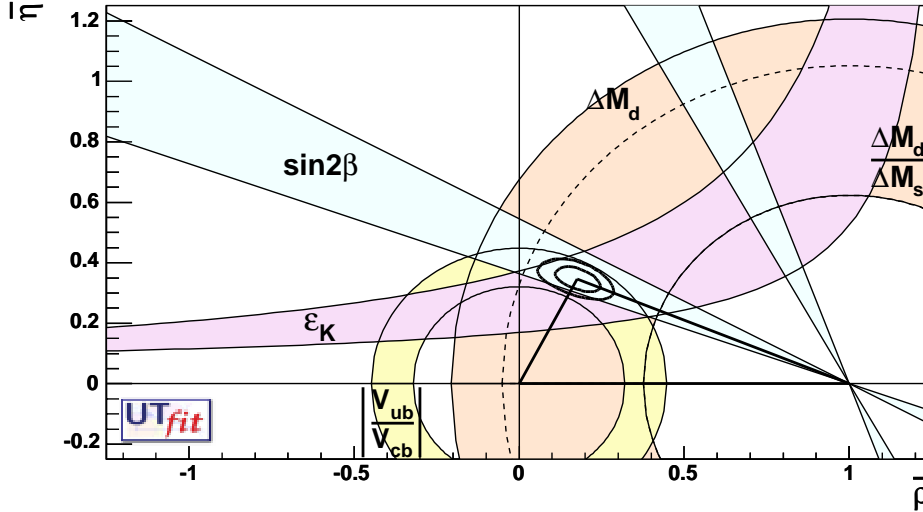


Figure 12: Allowed regions for $\bar{\rho}$ and $\bar{\eta}$ using the parameters listed in Table 3. The closed contours at 68% and 95% probability are shown. The full lines correspond to 95% probability regions for the constraints, given by the measurements of $|V_{ub}|/|V_{cb}|$, $|\varepsilon_K|$, Δm_d , Δm_s and $\sin(2\beta)$. The dotted curve corresponds to the 95% upper limit obtained from the experimental study of $B_s^0 - \bar{B}_s^0$ oscillations.

7.2.1 Indirect versus direct determination of the Unitarity Triangle angles

The value of $\sin(2\beta)$ was predicted, before its first direct measurement was obtained, by using all other available constraints, ($|V_{ub}|/|V_{cb}|$, $|\varepsilon_K|$, Δm_d and Δm_s). The “indirect”¹⁶ determination has improved regularly over the years. Figure 14 shows this evolution for the “indirect” determination of $\sin 2\beta$ which is compared with the recent determinations of $\sin(2\beta)$ from direct measurements.

This test should be repeated with other constraints.

The values for γ and $\sin 2\alpha$ given in Table 6 has to be taken as predictions for future measurements. A strong message is given for instance for the angle γ . The indirect determination of the angle γ is known

¹⁶in the following, for simplicity, we will note as “direct”(“indirect”), the determination of $\sin(2\beta)$ from $A_{CP}(J/\psi K^0)$ (other constraints).

with an accuracy of about 10%. It has to be stressed that, with present measurements, the probability that γ is greater than 90° is only 0.003%.

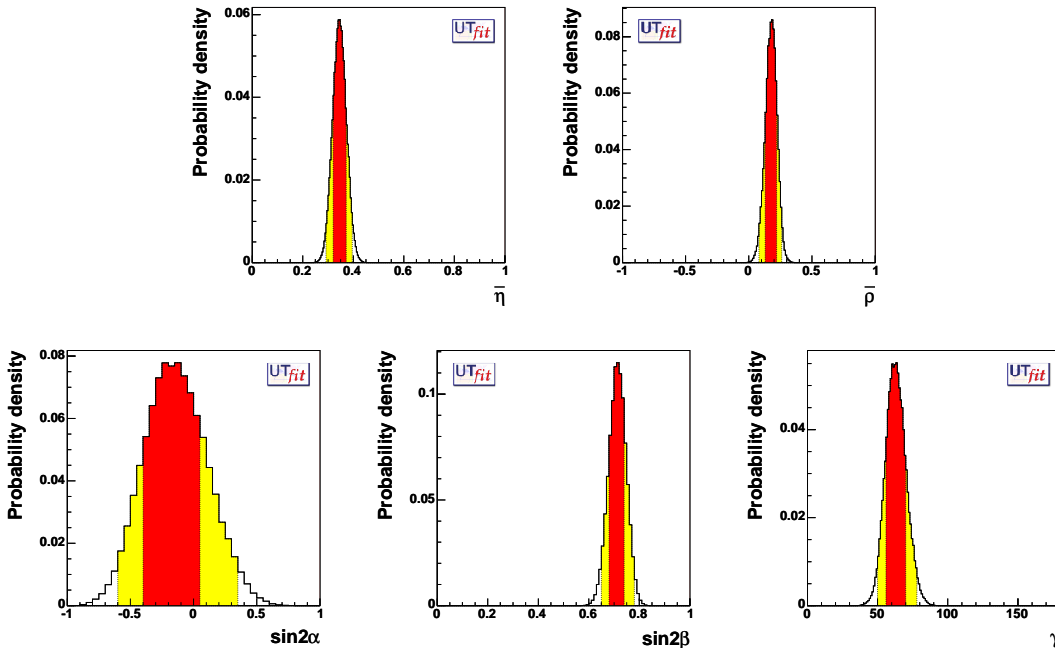


Figure 13: From top left to bottom, the p.d.f. for $\bar{\eta}$, $\bar{\rho}$, $\sin(2\alpha)$, $\sin(2\beta)$ and γ . The red (darker) and the yellow (clearer) zones correspond respectively to 68% and 95% of the normalised area. All available constraints have been used.

7.3 Determination of other important quantities

In previous sections we have seen that we can get distributions for the different unitarity triangle parameters and how it can be instructive to remove from the fitting procedure the external information on the value of one (or more) of the constraints.

In this section we get the distributions for the values of other quantities, entering into the Standard Model expressions for the constraints, such as the hadronic parameters, or of a constraint as Δm_s . In case of the hadronic parameters, for instance, it is instructive to remove, from the fit, in turn, their external information. The idea is to compare the uncertainty on a given quantity, determined in this way, to its present experimental or theoretical error. This comparison allows to quantify the importance of present determinations of the different quantities to define the limits of the allowed region for the unitarity triangle parameters.

7.3.1 The expected distribution for Δm_s

Figure 15 shows the allowed region for $\bar{\rho}$ and $\bar{\eta}$ obtained with all the constraints and how the constraint coming from the study of $B_s^0-\bar{B}_s^0$ mixing acts in this plane. A lower limit at 95% C.L. on Δm_s will exclude, at that degree of confidence, the $\bar{\rho}-\bar{\eta}$ region situated on the left of the corresponding curve.

It is also possible to extract the probability distribution for Δm_s , which is shown in Figure 16. Corresponding results are given in Table 7. Present analyses at LEP/SLD, with a sensitivity at 19.2 ps^{-1} are situated in a high probability region for a positive signal (as the “signal bump” appearing around 17.5 ps^{-1}).

Accurate measurements of Δm_s are thus expected soon from the TeVatron.

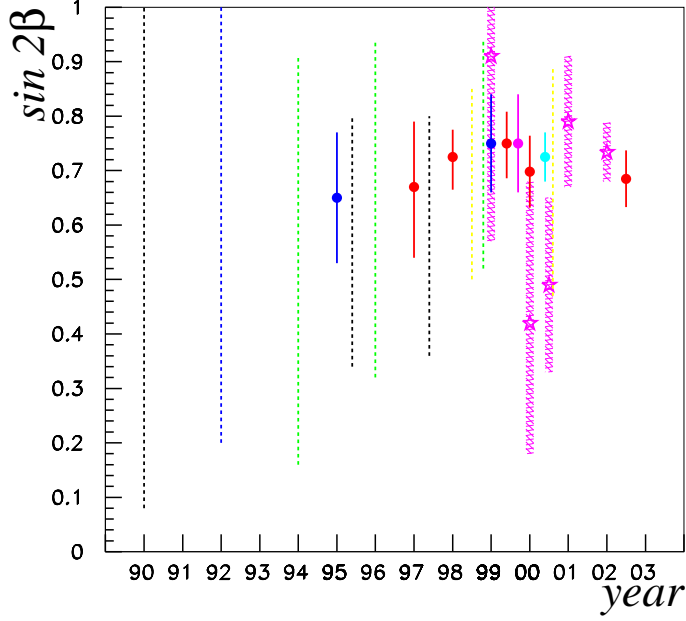


Figure 14: Evolution of the “indirect” determination of $\sin(2\beta)$ over the years. From left to right, they correspond to the following papers [38]: DDGN90, LMMR92, AL94, CFMRS95, BBL95, AL96, PPRS97, BF97, BPS98, PS98, AL99, CFGLM99, CPRS99, M99, CDFLMPRS00, B.et.al.00, HLLL00 and the value presented in this document. The dotted lines correspond to the 95% C.L. regions (the only information given in those papers). The larger bands (from year '99) correspond to values of $\sin(2\beta)$ from direct measurements ($\pm 1\sigma$).

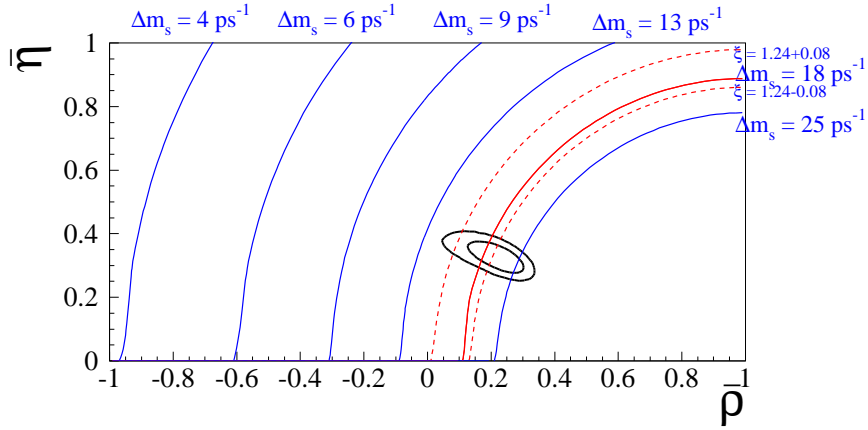


Figure 15: The allowed regions for $\bar{\rho}$ and $\bar{\eta}$ using the constraints given by the measurements of $|\varepsilon_K|$, $|V_{ub}|/|V_{cb}|$, Δm_d and $\sin(2\beta)$ at 68% and 95% probability are shown by the closed contour lines. The different continuous circles correspond to fixed values of Δm_s . Dashed circles, drawn on each side of the curve corresponding to $\Delta m_s = 18.0 \text{ ps}^{-1}$, indicate the effect of a variation by ± 0.08 on ξ .

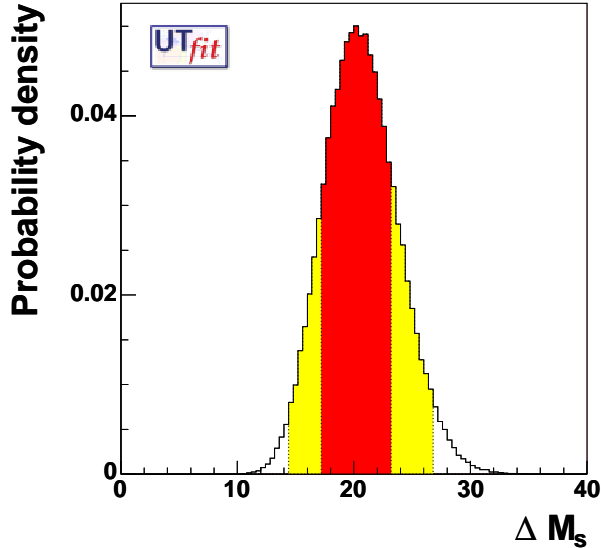


Figure 16: Δm_s probability distributions. The information from $B_s^0 - \bar{B}_s^0$ oscillations is not used.

Parameter	68%	95%	99%
Δm_s (including Δm_s) [ps^{-1}]	18.4 ± 1.6	(15.4-21.2)	(14.6-25.4)
Δm_s (without including Δm_s) [ps^{-1}]	20.2 ± 3.0	(14.4-26.8)	(13.2-29.2)

Table 7: Δm_s central values and ranges corresponding to defined levels of probability, obtained when including or not the information from the experimental amplitude spectrum $\mathcal{A}(\Delta m_s)$.

7.3.2 Determination of $f_{B_d} \sqrt{\hat{B}_{B_d}}$ and \hat{B}_K

The value of $f_{B_d} \sqrt{\hat{B}_{B_d}}$ can be obtained by removing¹⁷ the theoretical constraint coming from this parameter in the expression of the $B_d^0 - \bar{B}_d^0$ oscillation frequency Δm_d . The main conclusion of this study is that $f_{B_d} \sqrt{\hat{B}_{B_d}}$ is measured with an accuracy which is better than the current evaluation from lattice QCD, given in Section 6.4. Results are summarized in Table 8. This shows that the present CKM fit, when all the available constraints are used, is, in practice, weakly dependent on the exact value assumed for the uncertainty on $f_{B_d} \sqrt{\hat{B}_{B_d}}$.

Parameter	68%	95%	99%
$f_{B_d} \sqrt{\hat{B}_{B_d}}$ (MeV)	217 ± 12	(196-245)	(190-258)
\hat{B}_K	$0.69^{+0.13}_{-0.08}$	(0.53-0.96)	(0.49-1.09)

Table 8: Values and probability ranges for the non perturbative QCD parameters, if the external information (input) coming from the theoretical calculation of these parameters is not used in the CKM fits

¹⁷Technically we assume a uniform distribution in a range which is much larger than the possible values taken by the parameters.

The parameter \hat{B}_K can be also determined. Results are also summarized in Table 8. They indicate that values of \hat{B}_K smaller than 0.5 (0.3) correspond to 0.6% (5×10^{-6}) probability while large values of \hat{B}_K are compatible with the other constraints over a large domain. The present estimate of \hat{B}_K , from lattice QCD, with a 15% relative error (Table 3) has thus a large impact in the present analysis.

7.4 Evolution on the precision on $\bar{\rho}$ and $\bar{\eta}$ over the last 15 years

The evolution of our knowledge concerning the allowed region in the $(\bar{\rho}, \bar{\eta})$ plane is shown in Figure 17.

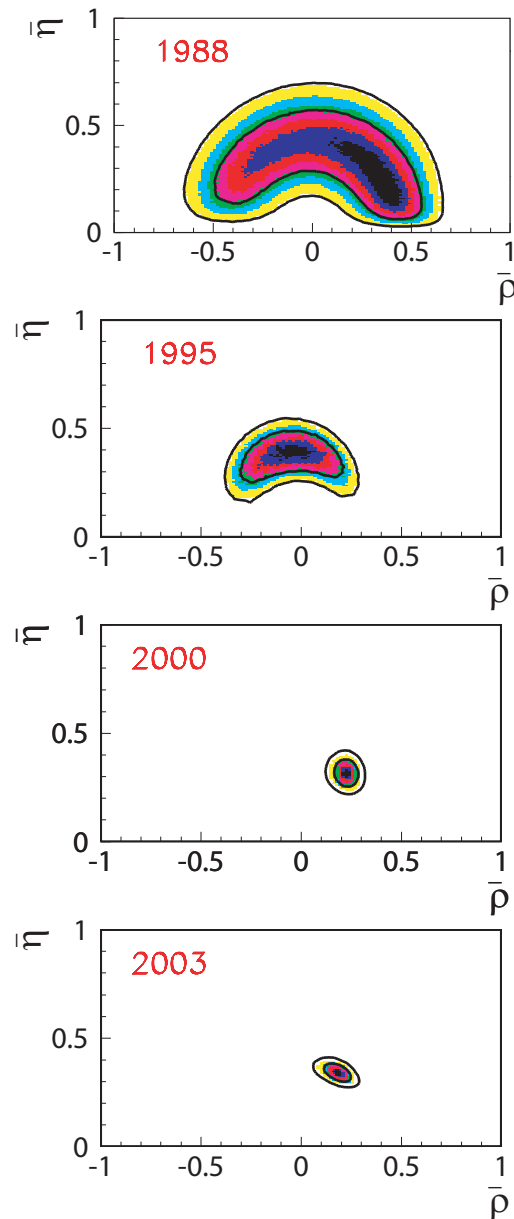


Figure 17: Evolution during the last 15 years of the allowed regions for $\bar{\rho}$ and $\bar{\eta}$ (contours at 68% and 95% probability are indicated). The very last results (updated till Winter 2004) are shown in Figure 12 and in Table 6.

The reduction of the size of these regions, from years 1995 to 2000, is essentially due to the measurements of the sides of the Unitarity Triangle and to the progress in OPE, HQET and lattice QCD theoretical parameters determinations. The additional reduction, from years 2000 to 2003, which mainly concerns $\bar{\eta}$, is essentially driven by the measurement of $\sin(2\beta)$ through the CP violation asymmetry in $J/\psi K^0$ decays.

7.5 Dulcis in fundo : the new-comers

The huge statistics collected the B-factories allow the measurements of new CP-violating quantities. Direct measurements of γ , $\sin(2\beta + \gamma)$ and $\sin 2\alpha$ are now available :

- determination of $\sin 2\alpha$ using charmless $\pi\pi$ events,
- determination of $\sin(2\beta + \gamma)$ using $D^{(*)}\pi$ events,
- determination of γ using DK events.

We do not enter in any details for these analyses which are described in U. Mallik lectures.

The Figure 18 shows the impact of these new measurements to provide additional constraints in the $\bar{\rho} - \bar{\eta}$ plane. More details are given in [46].

These plots show the potentialities of B-factories, considering that additional measurements will be available, in a near future (about 2 years), with more than four times the statistics.

8 Conclusions

Flavour physics in the quark sector is entered in its mature age. Many and interesting results have been produced during the last 15 years. Traditional main players (LEP/SLD/CLEO) delivered results until this year, while B factories are moving B studies into the era of precision physics.

Many quantities have already been measured with a good precision. $|V_{cb}|$ is today known with a relative precision better than 2%. In this case, not only, the decay width has been measured, but also some of the non-perturbative QCD parameters entering into its theoretical expressions. It is a great experimental achievement and a success of the theory description of the non-perturbative QCD phenomena in the framework of the OPE. Many different methods, more and more reliable, are now available for determining the CKM element $|V_{ub}|$. The relative precision, today, is of about 10% and will be certainly improved in a near future at B-factories. The time dependence behaviour of $B^0 - \bar{B}^0$ oscillations has been studied and precisely measured in the B_d^0 sector. The oscillation frequency Δm_d is known with a precision of about 1%. $B_s^0 - \bar{B}_s^0$ oscillations have not been measured sofar, but this search has pushed the experimental limit on the oscillation frequency Δm_s well beyond any initial prediction. Today we know that B_s^0 oscillate at least 30 times faster than B_d^0 mesons. The frequency of $B_s^0 - \bar{B}_s^0$ oscillations should be soon measured at the TeVatron. Nevertheless, the impact of the actual limit on Δm_s for the determination of the unitarity triangle parameters is crucial.

Many B decay branching fractions and relative CP asymmetries have been measured at B-factories. The outstanding result is the determination of $\sin 2\beta$ from B hadron decays into charmonium- K^0 final states. On the other hand many other exclusive hadronic rare B decays have been measured and constitute a gold mine for weak and hadronic physics, allowing to already extract different combinations of the unitarity triangle angles.

The unitarity triangle parameters are today known with a good precision. A crucial test has been already done: the comparison between the unitarity triangle parameters, as determined with quantities sensitive to the sides of the triangle (semileptonic B decays and oscillations), and the measurements of CP violation in the kaon (ϵ_K) and in the B ($\sin 2\beta$) sectors. The agreement is “unfortunately” excellent. The Standard Model is “Standardissimo”: it is also working in the flavour sector. This agreement is also an important test of the OPE, HQET and LQCD theories which have been used to extract the CKM parameters.

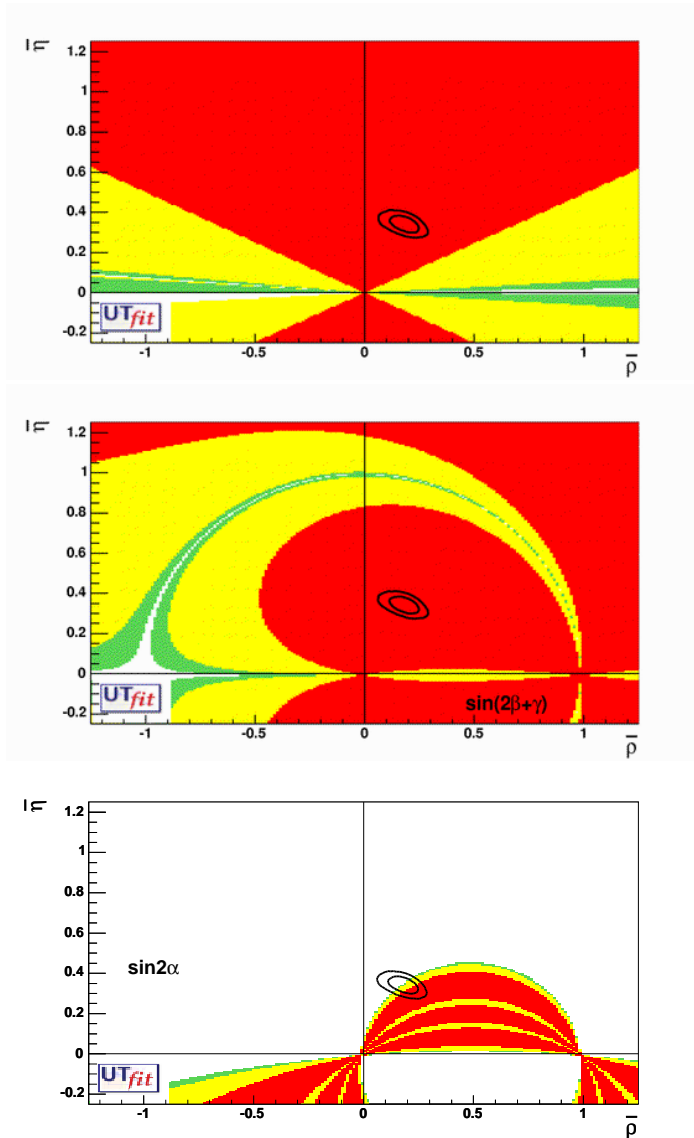


Figure 18: From top to bottom, the allowed region on the $\bar{\rho} - \bar{\eta}$ plane as selected by the direct measurement of γ , $\sin(2\beta + \gamma)$ and $\sin 2\alpha$. The red (darker), the yellow (clear) and green (clearer) zones correspond respectively to 68%, 95% and 99% of the normalised area. Contours at 68% and 95% probability selected using all the other available constraints are also shown.

The good news is that all these tests are at best at about 10% level. The current and the next facilities can surely push these tests to a 1% accuracy. It is important to note that charm physics can play an important role in this respect (providing a laboratory for LQCD) and the Charm-factory (CLEO-C) will play a central role for these issues.

9 Acknowledgements

I would like to thank the organizers, and especially Gerard Smadja, of the Cargèse School for the invitation and for having set up a very interesting school in a nice atmosphere.

I really would like to thank Vittorio Lubicz, Patrick Roudeau, Marie-Hélène Schune and Luca Silvestrini for the enlightening discussions and suggestions both in preparing these lectures and the document. Many thanks to Marcella Bona, Maurizio Pierini and Fabrizio Parodi, the “UT fitters” for providing me all the material for the determination of the CKM parameters.
 Merci à Catherine Bourge pour son aide.

References

- [1] N. Cabibbo, *Phys. Rev. Lett.* **10** (1963) 351.
- [2] M. Kobayashi and T. Maskawa, *Prog. Theor. Phys.* **49** (1973) 652.
- [3] A.J. Buras, M.E. Lautenbacher and G. Ostermaier, *Phys. Rev.* **D50** (1994) 3433.
- [4] C.M.G. Lattes, H. Muirhead, C.F. Powell and G.P. Occhialini, *Nature* **159**, 694 (1947).
- [5] G.D. Rochester and C.C. Butler, *Nature* **160**, 855 (1947).
- [6] L. Leprince-Ringuet and M. Lhéritier, *Comptes Rendues de l'Academie des Sciences* **219** (1944), 618. Presented à l'Académie de Sciences in the Séance du 17 Juin 1944.
- [7] R.W. Thompson et al. *Phys. Rev.* **83** (1951), 175.
- [8] M. Gell-Mann, *Phys. Rev.* **92** (1953), 833.
- [9] M. Gell-Mann, *Phys. Lett.* **8** (1964), 214.
- [10] G. Zweig, CERN-Report TH-401 (1964) and TH-412 (1964): published in *Developements in the Quark Theory of Hadrons, A Reprint Collection*, Vol I: 1964-1978, ed. by D.B. Lichtenberg and S.P. Rosen (Hadronic Press, Ma., 1980).
- [11] B.J. Bjorken and S.L. Glashow, *Phys. Lett.* **11** (1964) 255.
 Y. Hara, *Phys. Rev.* **B701** (1964) 134.
 Z. Maki and Y. Ohnuki, *Prog. Theor. Phys.* **32** (1964) 144.
- [12] S.L. Glashow, J. Iliopoulos and L. Maiani, *Phys. Rev.* **D2** (1970) 1285.
- [13] J.J. Aubert et al., BNL Spectrometer Coll., *Phys. Rev. Lett.* **33** (1974) 1404.
 J.E. Augustin et al., SPEAR Coll., *Phys. Rev. Lett.* **33** (1974) 1406.
- [14] V. Luth et al., SPEAR Coll., *Phys. Rev. Lett.* **34** (1975) 1125.
 G. Goldhaber et al., SPEAR Coll., *Phys. Rev. Lett.* **37** (1976) 255.
 I. Peruzzi et al., SPEAR Coll., *Phys. Rev. Lett.* **37** (1976) 569.
- [15] K. Niu, E. Mikumo and Y. Maeda, *Prog. Theor. Phys.* **46** (1971) 1644.
- [16] S. Bianco, F.L. Fabbri, D. Benson and I. Bigi hep-ex/0306039 to be published in *Il Nuovo Cimento*.
- [17] The story of the charm discovery in Japan : K. Niu *Proceed. of the First Intern. Workshop on Nucl. Emulsion Techn.* June 12-14, 1998, Nagoya, Japan (DPNU-98-39).
- [18] M.L. Perl et al., MARK I Coll., *Phys. Rev. Lett.* **35** (1975) 1489.
 M. L. Perl et al., MARK I Coll., *Phys. Lett.* **63B** (1976) 466.
- [19] S.W. Herb et al., Fermilab P.C. Coll., *Phys. Rev. Lett.* **39** (1977) 252.
 W. R. Innes et al., Fermilab P.C. Coll., *Phys. Rev. Lett.* **39** (1977) 1240.
- [20] C. Albjar et al., UA1 Coll., *Phys. Lett.* **B186** (1987) 247.
 H. Albrecht et al., ARGUS Coll., *Phys. Lett.* **B192** (1987) 245.
 A. Bean et al., CLEO Coll., *Phys. Rev. Lett.* **58** (1987) 183.

- [21] F. Abe *et al.*, CDF Collaboration, *Phys. Rev. Lett.* **74** (1995) 2626.
S. Abachi *et al.*, D0 Collaboration, *Phys. Rev. Lett.* **74** (1995) 2632.
- [22] L.L. Chau and W.-Y. Keung, *Phys. Rev. Lett.* **53** (1984) 1802.
- [23] K. Hagiwara *et al.*, Particle Data Group, *Phys. Rev.* **66** (2002) 010001.
- [24] L. Wolfenstein, *Phys. Rev. Lett.* **51** (1983) 1945.
- [25] M. Schmidtler and K.R. Schubert, *Z. Phys.* **C 53** (1992) 347.
- [26] T.Inami and C.S.Lim, *Prog.Theor.Phys.* **65** (1981) 297; *ibid.* **65** (1981) 1772.
- [27] A.J. Buras, M. Jasmin and P.H. Weisz, *Nucl. Phys.* **B347** (1990) 491.
- [28] S. Herrlich and U. Nierste, *Nucl. Phys.* **B419** (1994) 192;
G. Buchalla, A.J.Buras and M.E. Lautenbacher, *Rev. Mod. Phys.* **68**, (1996) 1125.
- [29] “THE CKM MATRIX AND THE UNITARITY TRIANGLE”. *Based on the First Workshop on “CKM Unitarity Triangle” held at CERN, 13-16 February 2002.* Edited by: M. Battaglia, A. Buras, P. Gambino and A. Stocchi. To be published as **CERN Yellow Book** (hep-ph/0304132).
- [30] Proceedings of the Second Workshop on “CKM Unitarity Triangle” *held in Durham, 5-9 April 2003.* Edited by: P. Ball, P. Kluit, J. Flynn and A. Stocchi.
- [31] <http://www.slac.stanford.edu/xorg/hfag/>
- [32] <http://www.hep.phys.soton.ac.uk/lwg-bmix/>
- [33] M. Ciuchini, E. Franco, V. Lubicz, F. Parodi, L. Silvestrini and A. Stocchi, “Unitarity Triangle in the Standard Model and sensitivity to new physics” (hep-ph/0307195)
- [34] M. Battaglia, M. Calvi, P. Gambino, A. Oyanguren, P. Roudeau, L. Salmi, J. Salt, A. Stocchi, N. Uraltsev “Heavy Quark Parameters and $|V_{cb}|$ from Spectral Moments in Semileptonic B Decays” **Phys. Lett.** **B556** (2003) 41-49 (hep-ph/0210319).
- [35] C. W. Bauer, Z. Ligeti, M. Luke, A. V. Manohar *Phys. Rev.* **D67** (2003) 054012. (hep-ph/0210027).
- [36] A. J. Buras, F. Parodi, A. Stocchi, “The CKM Matrix and The Unitarity Triangle: another Look” **JHEP** **0301** (2003) 029 (hep-ph/0207101).
- [37] M. Ciuchini, G. D’Agostini, E. Franco, V. Lubicz, G. Martinelli, F. Parodi, P. Roudeau, A. Stocchi, “2000 CKM-Triangle Analysis A Critical Review with Updated Experimental Inputs and Theoretical Parameters”, **JHEP** **0107** (2001) 013. (hep-ph/0012308).
- [38] C. Dib, I. Dumietz, F. Gilman, Y. Nir, *Phys. Rev.* **D41** (1990) 1522.
G. Buchalla, A.J. Buras and M.E. Lautenbacher, *Rev. Mod. Phys.* **68** (1996) 1125.
M. Lusignoli, L. Maiani, G. Martinelli and L. Reina, *Nucl. Phys.* **B369** (1992) 139.
A. Ali and D. London, in Proceeding of “ECFA Workshop on the Physics of a B Meson Factory”, Ed. R. Aleksan, A. Ali (1993);
A. Ali and D. London, hep-ph/9405283;
A. Ali and D. London, in Proceeding of “27th International Conference on High Energy Physics (ICHEP95)”, Glasgow, Scotland, 20-27 July 1994, hep-ph/9409399;
A. Ali and D. London, *Z. Phys.* **C65** (1995) 431. S. Herrlich and U. Nierste, *Phys. Rev.* **D52** (1995) 6505.
M. Ciuchini, E. Franco, G. Martinelli, L. Reina and L. Silvestrini, *Z. Phys.* **C68** (1995) 239.
A. Ali and D. London, *Nuovo. Cim.* **109A** (1996) 957;
A. Ali, *Acta Physica Polonica* **B 27** (1996) 3529;
A. Ali and D. London, *Nucl. Phys.* **54A** (1997) 297.

- A.J. Buras, Invited talk at “7th International Symposium on Heavy Flavour Physics”, Santa Barbara, CA, 7-11 July 1997, hep-ph/9711217;
- A.J. Buras and R. Fleischer, *Adv. Ser. Direct. High. Energy Phys.* **15** (1998) 65; hep-ph/9704376.
- R. Barbieri, L.J. Hall, S. Raby and A. Romanino, *Nucl. Phys.* **B493** (1997) 3.
- A. Ali and B. Kayser, invited article in “The Particle Century”, Inst. of Physics Publ., Inc., Bristol and Philadelphia, 1998, Ed. Gordon Fraser, hep-ph/9806230.
- P. Paganini, F. Parodi, P. Roudeau and A. Stocchi, *Phys. Scripta* **V. 58** (1998) 556.
- F. Parodi, P. Roudeau and A. Stocchi, *Nuovo Cim.* **112A** (1999) 833.
- F. Caravaglios, F. Parodi, P. Roudeau, A. Stocchi, hep-ph/0002171, talk at “B_{CP} 99”, Taipei, Taiwan Dec. 3-7 1999, to appear in the Proceedings.
- S. Mele, *Phys. ReV.* **D59** (1999) 113011.
- A. Ali and D. London, *Eur. Phys. J.* **C9** (1999) 687.
- S. Plaszczynski, M.H. Schune, Talk given at Heavy Flavours 8, Southampton, UK, 1999 (hep-ph/9911280).
- M. Ciuchini, E. Franco, L. Giusti, V. Lubicz and G. Martinelli, *Nucl. Phys.* **B573** (2000) 201.
- M. Bargiotti *et al.*, *La Rivista del Nuovo Cimento* **Vol. 23N3** (2000) 1.
- [39] L. Lellouch, Plenary Talk given at the 31st ICHEP, Amsterdam, The Netherlands, July 24th-31st, 2002.
- [40] A. S. Kronfeld, P. B. Mackenzie, J. N. Simone, S. Hashimoto, S. M. Ryan, proceedings of FPCP, May 16–18, Philadelphia, Pennsylvania; *Phys. ReV.* **D66** (2002) 014503. (hep-ph/0110253).
- [41] A. Stocchi “Experimental Results on Heavy Quarks” Plenary talk at ICHEP02 (26-31/7/2002 Amsterdam) *Nucl. Phys. Proc. Suppl.* **117** (2003) 145-163 (hep-ph/0211245).
M. Battaglia, talk given at ICHEP02 (26-31/7/2002 Amsterdam, The Netherlands)
- [42] H.G. Moser and A. Roussarie, *Nucl. Instum. Meth.* **A384** (1997) 491.
- [43] K. G. Wilson *Phys. ReV.* **D10** (1974), 2445.
- [44] JLQCD Coll., S. Hashimoto et al., hep-lat/0209091.
- [45] A.S. Kronfeld and S.M. Ryan, *Phys. Lett* **B543** (2002) 59, hep-ph/0206058.
- [46] <http://www.utfit.org>
(the UTfit group : M. Bona, M. Ciuchini, G. D’Agostini, E. Franco, V. Lubicz, G. Martinelli, F. Parodi, M. Pierini, P. Roudeau, C. Schiavi, L. Silvestrini, A. Stocchi)